

THESIS

ANALYSIS AND CONTROL CO-DESIGN OPTIMIZATION OF NATURAL GAS POWER
PLANTS WITH CARBON CAPTURE AND THERMAL ENERGY STORAGE

Submitted by

Roberto Vercellino

Department of Mechanical Engineering

In partial fulfillment of the requirements

For the Degree of Master of Science

Colorado State University

Fort Collins, Colorado

Summer 2022

Master's Committee:

Advisor: Daniel R. Herber

Co-Advisor: Todd M. Bandhauer

Jason C. Quinn

Timothy C. Coburn

Copyright by Roberto Vercellino 2022

All Rights Reserved

ABSTRACT

ANALYSIS AND CONTROL CO-DESIGN OPTIMIZATION OF NATURAL GAS POWER PLANTS WITH CARBON CAPTURE AND THERMAL ENERGY STORAGE

In this work, an optimization model was constructed to help address important design and operation questions for a novel system combining natural gas power plants (NGCC) with carbon capture (CC) and hot and cold thermal energy storage (TES) units. The conceptualization of this system is motivated by the expected evolution of the electricity markets towards a carbon-neutral electricity grid heavily penetrated by renewable energy sources, resulting in highly variable electricity prices and demand. In this context, there will be an opportunity for clean, flexible, and cheap fossil fuel-based generators, such as NGCC plants with CC, to complement renewable generation. However, while recent work has demonstrated that high CO₂ rates are achievable, challenges due to high capital costs, flexibility limitations, and the parasitic load imposed by CC systems onto NGCC power plants have so far prevented its commercialization. Coupling TES units with CC and NGCC would allow to store thermal energy into the TES units when the electricity prices are low, either by subtracting it from the NGCC or by extracting it from the grid, and to discharge thermal power at peak prices, from the hot storage (HS) to offset the parasitic load of the CC system and from the cold storage (CS) for chilling the inlet of the NGCC combustion turbine and increase the output of the cycle beyond nominal value. For the early-stage engineering studies investigating the feasibility of this novel system, a control co-design (CCD) approach is taken where key plant sizing decisions (including storage capacities and energy transfer rates) and operational control (e.g., when to store and use thermal energy and operate the power plant) are considered in an integrated manner using a simultaneous CCD strategy. The optimal design, as well as the operation of the system, are determined for an entire year (either all-at-once or through a moving prediction horizons strategy) in a large, sparse linear optimization problem. The results demonstrate both the

need for optimal operation to enable a fair economic assessment of the proposed system as well as optimal sizing decisions due to sensitivity to a variety of scenarios, including different market conditions, site locations, and technology options. After detailed analysis, the technology shows remarkable promise in that it outperforms NGCC power plants with state-of-the-art CC systems in many of the scenarios evaluated. The best overall TES technology solution relies on cheap excess grid electricity from renewable sources to charge the TES units – the HS via resistive heating and the CS through an ammonia-based vapor compression cycle. Future enhancements to the optimization model are also discussed, which include additional degrees of freedom to the CC system, adapting the model to evaluate other energy sources and storage technologies, and considering uncertainty in the market signals directly in the optimization model.

ACKNOWLEDGEMENTS

At the outset of this thesis, I would like to acknowledge the people and organizations who have supported me throughout my personal, academic and professional journey and without whom this work would not have been possible. First, I would like to thank my advisor, Prof. Daniel Herber, who for more than two years has shown continuous support, patience and trust, pushing me to my limits and guiding me through the challenge of overcoming them. I would also like to acknowledge the rest of my thesis committee: Profs. Todd Bandhauer, Jason Quinn, and Timothy Coburn for their precious time and valuable recommendations aiming at improving the quality of my work.

I could not have achieved this or many other these goals without my family, whose warm affection and support never fail to motivate me and fill me with gratitude, despite the distance. I would also like to give a special mention to Lena, my partner, for her unfailing support, patience and understanding throughout this journey: I could not imagine a better person with whom to share my life.

I would also like to acknowledge the other members of the wonderful research team who have also worked on this project, whose extraordinary abilities, motivation and personability allowed the team to consistently move forward and achieve outstanding results. Specifically, I would like to mention Ethan Markey, for his contribution to the thermodynamic models of the thermal storage technology; Braden Limb, for the remarkable leadership demonstrated in managing the team and developing the economic model used in this work; Joe Huyett, Max Pisciotta, Shane Garland and Profs. Todd Bandhauer, Daniel Herber, Jason Quinn and Pete Psarras for guiding the team towards the success in this project.

Finally I would like to acknowledge the many brilliant co-workers who with time have become long-lasting friends: Athul Sundarajan, Saeed Azad, Tomas Auruskevicius, Ben Platt, Abe Darden, Dylan Giardina, John Flynn, Brye Windell and many others. The daily interactions at work and the many other experiences shared with them not only have substantially contributed to my growth as a scientist, but as a person too.

DEDICATION

To my family,

Thank you.

TABLE OF CONTENTS

ABSTRACT	ii
ACKNOWLEDGEMENTS	iv
DEDICATION	v
LIST OF TABLES	viii
LIST OF FIGURES	ix
LIST OF ACRONYMS	x
LIST OF SYMBOLS	xi
Chapter 1 Introduction	1
1.1 The Climate Crisis and Its Effects on the Energy Market	1
1.2 Natural Gas Combined Cycle Power Plants	3
1.3 Post-Combustion Carbon Capture	5
1.4 Coupling Thermal Energy Storage with Carbon Capture	7
1.5 Control Co-design Optimization	11
1.6 Research Questions	13
1.7 Summary and Thesis Content	14
Chapter 2 Optimization Problem Formulation and Strategy	15
2.1 Problem Formulation	15
2.1.1 Thermal Energy Storage	15
2.1.2 Natural Gas Combined Cycle Power Plant	18
2.1.3 Carbon Capture	20
2.1.4 Electricity Generation	22
2.1.5 Techno-Economic Analysis	23
2.1.6 Objective Function and Summary	26
2.2 Optimization Strategy Considerations	27
2.2.1 Approximations	28
2.2.2 Problem Discretization	28
2.2.3 Moving Prediction Horizons	29
Chapter 3 Results and Discussion	32
3.1 Control Strategy Results	33
3.2 Justifications for Open-loop Control Co-design	36
3.3 Temperature-dependence Results	39
3.4 Moving Prediction Horizons Strategy Results	41
3.5 TES Technology Comparison Results	42
Chapter 4 Conclusion	46
4.1 Summary	46
4.2 Future Work	47

Bibliography	50
Appendix A Case Study Parameters	58
A.1 NPV Economic Assumptions	58
A.2 Technology Parameters	58
Appendix B Extended Time Horizon Visualizations	60

LIST OF TABLES

1.1	Comparison in LCOE, CO ₂ emissions, and flexibility between major energy generation technologies [1–4].	4
1.2	Parameters comparison between an NGCC power plant with (B31A) and without PCC (B31B) [1].	6
1.3	Several TES configurations and their working principles, as presented in [5,6].	10
A.1	Economic assumptions for the calculation of net present value in the case studies.	58
A.2	Techno-economic parameters for the technology configurations examined in the case studies.	59

LIST OF FIGURES

1.1	The comparison between a snippet of electricity prices from the month of April 2022 and a prediction for 2030 shows an expected increase in prices variability.	2
1.2	Data from the U.S. Energy Information Administration show net generation from NGCC power plants have steadily increased, a trend that is expected to continue in the near future.	3
1.3	Illustration of (a) CO ₂ solvent-based absorber and (b) stripper for solvent regeneration [7] used for post combustion CO ₂ capture.	5
1.4	Simplified diagram of the different operation modes of TES units coupled with an NGCC plant and PCC [5].	8
1.5	Simplified operation of the TES in response to variable electricity prices.	9
1.6	Illustration of the two fundamental CCD strategies [8].	12
2.1	Key subsystems and the flows between them.	16
2.2	Overview of the nested control co-design optimization architecture for the moving prediction horizons approach.	30
2.3	Moving prediction horizons and control window illustration.	30
3.1	Snippet of an entire year’s solution illustrating the control, states, and net power output.	33
3.2	The optimization results show certain correlation between typical operational modes of the system and the electricity prices.	35
3.3	A comparison with an heuristic-based control strategy shows the benefits of the optimization-based approach in handling specific situations (a), and returning more accurate results (b).	37
3.4	Motivation for open-loop control co-design optimization.	38
3.5	CS boosting operation for two different locations demonstrating temperature-dependent optimal operation.	40
3.6	Comparing optimal net present value results for several locations and correlating them with their mean temperatures.	41
3.7	Illustration of the moving prediction horizon approach with a prediction window of 6 hours and control window of 3 hours.	42
3.8	Net present value results for various prediction horizon and control window lengths in the moving prediction horizon approach compared to the maximum NPV for this scenario.	43
3.9	Comparing three different system configurations under several market scenarios including (a) net present value; (b) optimal storage capacities Σ_{HS} and Σ_{CS} ; (c) optimal TES charging power penalties $P_{HS,in}$ and $P_{HS,in}$; and (d) equivalent optimal thermal energy transfer to the TES units.	44
B.1	Control signals for optimal TES operation for 20 days in February.	60
B.2	Control signals for optimal TES operation for 20 days in May.	61
B.3	Control signals for optimal TES operation for 20 days in August.	61
B.4	Control signals for optimal TES operation for 20 days in November.	62

LIST OF ACRONYMS

Term	Description	On page(s)
CC	Carbon capture	5–11, 13–17, 20–22, 24, 32, 35–37, 40–42, 46–48
CS	Cold thermal energy storage	7–11, 13, 15–17, 20–22, 24, 27, 33–40, 42–45, 47, 60
HS	Hot thermal energy storage	7–11, 13, 15–17, 20, 22, 24, 27, 33–35, 37–39, 42–45, 47, 48, 60
NGCC	Natural gas combined cycle	ix, 3, 4, 6–11, 13–15, 18–20, 27, 32, 36, 37, 39, 41–43, 46–48
PP	Power plant	3, 7–10, 15, 17–24, 27, 34–36, 39, 40, 42, 43, 48
TES	Thermal energy storage	ix, 7–11, 13–20, 22–24, 27, 28, 32, 34–47, 60–62
CCD	Control co-design	ix, 11–13, 15, 26, 27, 30, 31, 36, 38, 45, 49
DAC	Direct air capture	5
DT	Direct transcription	28
EIA	Energy Information Administration	1
GHG	Green house gasses	1, 4
LCOE	Levelized cost of electricity	viii, 1, 4, 6, 24
LTI	Linear time-invariant	27
LTV	Time-varying linear	29
MPC	Model predictive control	29
MPH	Moving prediction horizons	41, 42
NETL	National Energy Technology Laboratory	32, 42
NPV	Net present value	ix, 15, 22, 24–30, 32, 33, 40–43, 48, 58
NREL	National Renewable Energy Laboratory	32
PCC	Post-combustion carbon capture	viii, ix, 4–8
ZOH	Zero-order hold	28

LIST OF SYMBOLS

Term	Description	On page(s)
C_{CC}	Total fixed capital cost to realize the carbon capture subsystem	24
C_{CS}	Total capital cost to realize the cold storage unit	24
C_{FOM}	Instantaneous fixed operation and maintenance costs for each of the subsystems	23, 24
C_{HS}	Total capital cost to realize the hot storage unit	24
C_{cap}	Total capital costs of the system	24
C_{PP}	Total fixed capital cost to realize the natural gas power plant	24
C_{VOM}	Instantaneous variable operation and maintenance costs depending on running each of the subsystems	23
DF	Economic discount factor	25
$E_{CS,0}$	Initial cold storage unit level	18
E_{CS}	State optimization variable representing the cold storage unit level	18, 27
$E_{HS,0}$	Initial hot storage unit level	18
E_{HS}	State optimization variable representing the hot storage unit level	18, 27
IRR	Internal rate of return	25
L_t	Loan term representing the system's lifetime	25
NPV	Net present value	25, 27
P_{CCE}	Electrical power requirement to run the carbon capture subsystem	21, 22
P_{CCT}	Thermal power requirement to run the carbon capture subsystem	21, 22
$P_{CS,in}$	Plant design optimization variable representing the maximum cold thermal energy charging power	15, 16, 26
$P_{CS,out}$	Plant design optimization variable representing the maximum cold thermal energy discharging power	15, 16, 26
$P_{HS,in}$	Plant design optimization variable representing the maximum hot thermal energy storage charging power	15, 16, 26
$P_{HS,out}$	Plant design optimization variable representing the maximum hot thermal energy storage discharging power	15, 16, 26
$P_{PP,0}$	Initial natural gas plant power level	19
T_0	Ambient temperature	15, 27
T_{year}	Integral upper bound representing a full year of operation	25, 26
V_{exp}	Annual total expenses of the system	25
V_{income}	Income generated over the system's lifetime	25, 26
V_{rev}	Annual total revenue of the system	25
Δc_d	Decrease in carbon capture percentage when the cold storage is discharged	20
$\Delta \rho_{C,in}$	Coefficient describing the linear trajectory of the carbon captured by the system from the neutral operation mode to the maximum discharging of the cold storage	21

Term	Description	On page(s)
$\Delta\rho_{C,out}$	Coefficient describing the linear trajectory of the carbon emitted into the atmosphere by the system from the neutral operation mode to the maximum discharging of the cold storage	21
$\Delta\rho_f$	Conversion factor determining the fuel consumed by discharging the cold storage unit per unit power output	20
Σ_{CS}	Plant design optimization variable representing the maximum cold thermal energy storage capacity	15, 16, 26
Σ_{HS}	Plant design optimization variable representing the maximum hot thermal energy storage capacity	15, 16, 26
α_C	Conversion coefficient from fuel burned to carbon generated	20, 21
β_C	Instantaneous carbon capture rate	20
ξ	Plant state optimization variables	27
p	Plant design optimization variables	15, 26, 27
u_P	Plant control optimization variables administering the natural gas power plant	18
u_T	Plant control optimization variables administering the thermal storage units	17
u	Plant control optimization variables	27
η_{CS}	Efficiency losses for discharging the cold storage unit	22
η_{HS}	Efficiency losses for discharging the hot storage unit	22
η_{GE}	Efficiency of conversion from thermal to electrical power	22
$\hat{m}_{C,in}$	Linearized instantaneous carbon captured by the system	21
$\hat{m}_{C,out}$	Linearized instantaneous carbon emitted into the atmosphere by the system	21
$\kappa_{CS,in}$	Coefficient of conversion from electricity to equivalent thermal power charging the cold storage	18
$\kappa_{CS,out}$	Coefficient of conversion from electricity to equivalent thermal power discharging from cold storage	18
$\kappa_{HS,in}$	Coefficient of conversion from electricity to equivalent thermal power charging the hot storage	18
$\kappa_{HS,out}$	Coefficient of conversion from electricity to equivalent thermal power discharging from hot storage	18
μ_f	Temperature-dependent efficiency affecting the fuel consumption of the natural gas plant	20
$\mu_{\Delta c}$	Temperature-dependent efficiency affecting the decrease in carbon capture rate from discharging the cold storage	20
$\mu_{\Delta f}$	Temperature-dependent efficiency affecting the fuel consumption of the discharging the cold storage	20
$\mu_{CS,in}$	Temperature-dependent efficiency for charging the cold storage unit	17
$\mu_{CS,out}$	Temperature-dependent efficiency for discharging the cold storage unit	17
$\mu_{HS,in}$	Temperature-dependent efficiency for charging the hot storage unit	17

Term	Description	On page(s)
$\mu_{HS,out}$	Temperature-dependent efficiency for discharging the hot storage unit	17
μ_{PP}	Temperature-dependent efficiency for the output power from the natural gas plant	19
μ_c	Temperature-dependent efficiency affecting the nominal carbon capture rate	20
τ_{PP}	Time constant for the ramp rate of effective power output from the natural gas plant	19
$\bar{P}_{CS,in}$	Upper bound on maximum cold thermal energy storage charging power	17
$\bar{P}_{CS,out}$	Upper bound on maximum cold thermal energy storage discharging power	16
$\bar{P}_{HS,in}$	Upper bound on maximum hot thermal energy storage charging power	17
$\bar{P}_{HS,out}$	Upper bound on maximum hot thermal energy storage discharging power	16
\bar{P}_{PP}	Maximum nominal power output from the natural gas plant	19
$\bar{\beta}_C$	Nominal carbon capture rate	21, 22
$\rho_{C,in}$	Carbon captured by the system in neutral operation mode	21
$\rho_{C,out}$	Carbon emitted into the atmosphere by the system in neutral operation mode	21
P_{AUX}	Auxiliary electrical power requirements	22
P_G	Effective power delivered to the grid	22
P_{PCT}	Thermal power extracted from the natural gas plant to run the carbon capture subsystem	22
P_{PE}	Gross electricity generated by the system	22
P_{TH}	Corrected thermal power output of the system	22
$c_{CC,FOM}$	Instantaneous fixed operation cost for the carbon capture subsystem	24
$c_{CC,VOM}$	Instantaneous variable operation cost for the carbon capture subsystem per unit carbon captured	23
c_{CO_2}	Selected carbon tax	23
$c_{CS,FOM}$	Instantaneous fixed operation cost for the cold storage system per unit power capacity realized	24
$c_{CS,TES,FOM}$	Instantaneous fixed operation cost per unit cold storage capacity realized	24
$c_{CS,TES}$	Capital cost per unit cold storage capacity	24
$c_{CS,VOM}$	Instantaneous variable operation cost for the cold storage system per unit power displaced	23
$c_{HS,FOM}$	Instantaneous fixed operation cost for the hot storage system per unit power capacity realized	24
$c_{HS,TES,FOM}$	Instantaneous fixed operation cost per unit hot storage capacity realized	24
$c_{HS,TES}$	Capital cost per unit hot storage capacity	24

Term	Description	On page(s)
$c_{HS,VOM}$	Instantaneous variable operation cost for the hot storage system per unit power displaced	23
$c_{CS,in}$	Capital cost of the cold storage unit per unit charging capacity	24
$c_{CS,out}$	Capital cost of the cold storage unit per unit discharging capacity	24
$c_{HS,in}$	Capital cost of the hot storage unit per unit charging capacity	24
$c_{HS,out}$	Capital cost of the hot storage unit per unit discharging capacity	24
c_{elec}	Instantaneous electricity market price	23
c_{fuel}	Instantaneous fuel market price	23
$c_{PP,FOM}$	Instantaneous fixed operation cost for the natural gas plant	24
$c_{PP,VOM}$	Instantaneous variable operation cost for the natural gas plant per unit power generated	23
i_e	Expected annual percent change in the electricity prices	25
i_f	Expected annual percent change in the fuel prices	25
$p_{CS,in}$	Control decision to charge the cold storage unit	17, 22, 27
$p_{CS,out}$	Control decision to discharge the cold storage unit	17, 27
$p_{HS,in}$	Control decision to charge the hot storage unit	17, 22, 27
$p_{HS,out}$	Control decision to discharge the hot storage unit	17, 27
p_{PP}	Control decision representing the requested power from the natural gas plant	18, 27
t	Time	15, 27
v_{exp}	Instantaneous expenses for running the system	23
v_{fuel}	Instantaneous cost of fuel for running the system	23, 25
v_{op}	Instantaneous non-fuel operation costs for running the system	23, 25
v_{rev}	Instantaneous revenue generated by the system	23, 25
y	Year	25
P_{PP}	State optimization variable representing the effective power output from the natural gas plant	19, 27
ρ_f	Conversion factor determining the fuel consumed by the natural gas plant per unit power output	20
c_n	Nominal carbon capture rate in neutral operation mode	20
m_f	Instantaneous fuel consumption of the system	20
$m_{C,in}$	Instantaneous carbon captured by the system	21
$m_{C,out}$	Instantaneous carbon emitted into the atmosphere by the system	21

Chapter 1

Introduction

1.1 The Climate Crisis and Its Effects on the Energy Market

The increasing concentration of green house gasses (GHG) in the Earth's atmosphere has contributed to adverse changes to the global climate, which include an increase in the average surface temperature by 1°C, an increase in the average ocean temperature by 0.33°C, shrinking of the ice sheets, ocean level rising and acidification, and an increase of extreme weather events [7, 9]. These changes constitute a threat not only to Earth's biosphere but also to humankind, and they are largely due to the emission of GHG in the atmosphere due to humans' increasing industrial activities [9, 10]. Policymakers have reached international agreements to drastically reduce GHG emissions and arrive at "net-zero" by 2050 [11]. The energy sector accounts for around 75% of the total GHG emissions, which are mainly due to the combustion of fossil fuel-based power plants [12]. In its effort towards net-zero, the United States has pledged to erase all GHG from the energy sector by 2035 [13]. The strategy to achieve this goal includes increasing economic penalties associated with the emission of GHG in the form of a "carbon tax", and ultimately moving towards an energy sector dominated by renewable energy resources like solar, wind, bio, geothermal, and hydro energy, coupled with energy storage [12].

While U.S. fossil fuel-based energy generation still constitutes the dominating energy source, wind and solar as renewable sources prevail in terms of added capacity, a trend that is expected to increase in the foreseeable future as the cost of electricity provided by these resources continues to decrease [14]. In particular, the U.S. Energy Information Administration (EIA) indicated that solar power will account for 46% (21.5 GW), wind for 17% (7.6 GW), and batteries 11% (2.2 GW) of new planned generation capacity, while coal plants will account for 85% (12.6 GW) of retired generating capacity in 2022 [15, 16]. While the levelized cost of electricity (LCOE) for wind and solar continues to decrease, their increasing penetration will radically change the nature of the

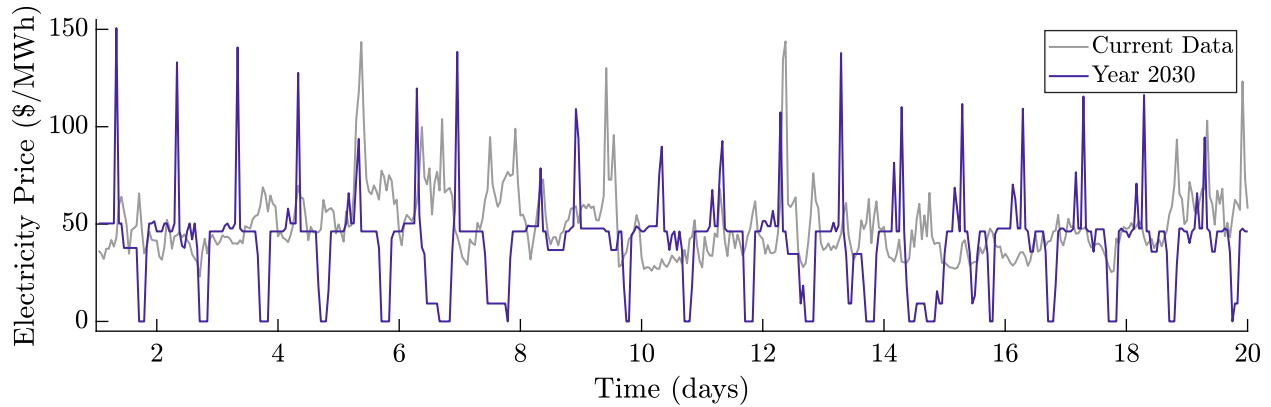


Figure 1.1: The comparison between a snippet of electricity prices from the month of April 2022 and a prediction for 2030 shows an expected increase in prices variability.

electricity markets [17]. In fact, because wind and solar are by nature passive energy resources – their electricity generation strictly depends on current environmental conditions – issues related to unreliability and intermittency of these sources raise concerns about their ability to fully satisfy an ever-increasing electricity demand. These concerns are to be reflected in the electricity market in the form of increasing electricity price, but more importantly, an increase in their variability [18]. For instance, Fig. 1.1 shows a snippet of hourly electricity prices from the state of New York for April 2022, compared with a prediction for 2030 made for the same area by the capacity expansion model GenX [19]. While the average electricity price in this scenario is higher for the current data than it is predicted in the future – 48.6 \$/MWh in the current age and 39.3 in 2030 – the standard deviation of the future data is much higher compared with the present – 25.5 compared to 19.2. The increased future variability is also clear from the image, where it can be seen how, on a daily basis, the prices go from almost 0 \$/MWh – presumably because of renewable sources over-generation – to nearly 150 \$/MWh – likely because the same renewable sources are offline.

The gap left by intermittent renewable sources in the electricity demand is expected to be filled by alternative generation sources, which will need to be readily available and flexible to quickly ramp up generation, cheap enough to be competitive in the market, as well as carbon-neutral (or close enough), to comply with CO₂ policies [17, 20, 21].

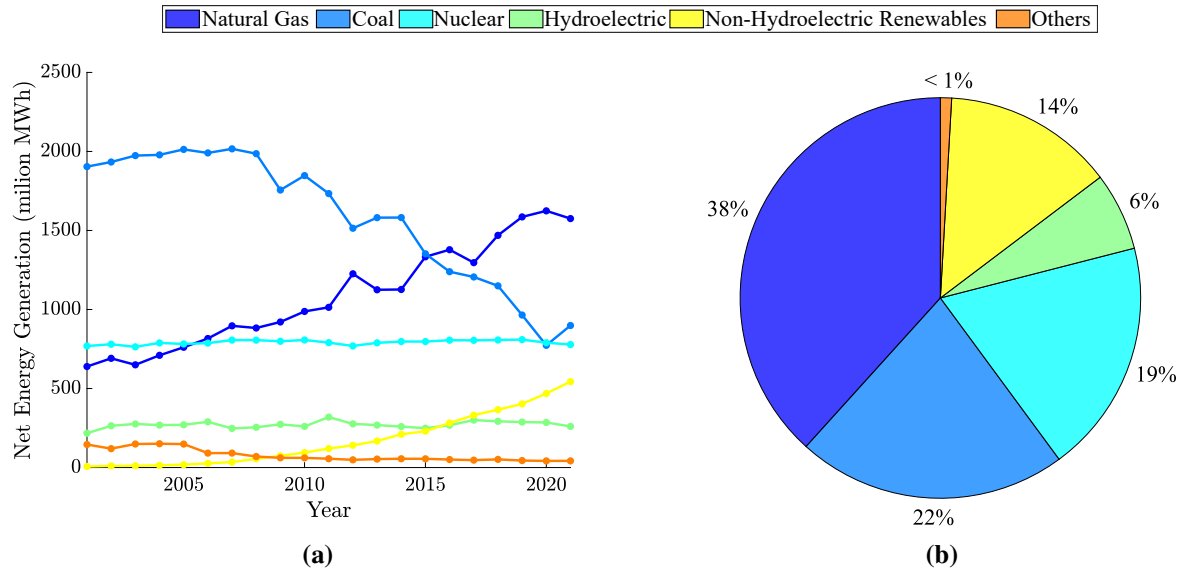


Figure 1.2: Data from the U.S. Energy Information Administration show net generation from NGCC power plants have steadily increased, a trend that is expected to continue in the near future.

1.2 Natural Gas Combined Cycle Power Plants

Natural gas combined cycle (NGCC) power plant (PP) in the U.S. are currently the largest source of energy. For instance, Fig. 1.2b shows how in 2021 38% of the net energy generation of the U.S. came from NGCC plants [22]. In 2022, NGCC plants also account for 21% of new planned capacity (9.6 GW) [16]. This is part of an ongoing trend that has seen the natural gas infrastructure substantially grow since the early 2000s, as is shown in Fig. 1.2a. This growth is expected to continue in the near future, although in the long-term it is not clear how the natural gas infrastructure will be integrated within electricity markets dominated by renewable sources [23].

As suggested by the name, NGCC power plants combine two power generation cycles, in which waste heat from the topper cycle is extracted and used within a bottomer cycle to generate additional power [24]. From a high level, these are the fundamental steps in NGCC power plants: 1) natural gas is combusted to aliment a Brayton cycle in which power is generated through expansion in a gas turbine; 2) waste heat is extracted from the exhaust of the turbine and used to generate steam in a large, multi-stage heat exchanger, referred to as a heat recovery steam generator (or HRSG); 3) the steam at different stages is expanded in a series of steam turbines for additional power [25]. Through the combination of Brayton and Rankine cycles, combined cycles

Table 1.1: Comparison in LCOE, CO₂ emissions, and flexibility between major energy generation technologies [1–4].

Parameters	Units	Resource				
		Coal	Gas Turbine	NGCC	Nuclear	Hydroelectric
Capacity Factor	%	85	10	87	90	54
LCOE	\$/MWh net	82.6	117.9	39.9	88.2	64.3
CO ₂ Emission	lb/MWh net	1714	1150	755	–	–
Ramp Rate	%/min	6	20	18	2	15
Start Up Time (Hot Start)	hr	3	0.16	0.5	–	0.1

can achieve thermodynamic efficiencies as high as 60%, with most NGCC power plants ranging between 45% and 57% [25].

Experts state that NGCC power plants will continue to play a significant role in future low-carbon energy markets, even though renewable sources will fulfill a considerable fraction of the base-load [21,23,26]. The position that NGCC plants would play in that scenario consists of filling periods of high unsatisfied demand, when renewable energy sources are unable to fulfill it [21,26]. Table 1.1 shows a comparison between some of the most prevalent generation sources in the current US market. By consulting the overall performance of NGCC power plants, which show by far the lowest levelized cost of electricity (LCOE) among the technologies reported, it becomes more clear why this resource is currently prevalent. With the perspective of future markets determined by low-carbon policies, NGCC power plants show CO₂ emissions that are 55% less than coal and 24% less than gas-fired peaking turbines. While gas peaking turbines exhibit remarkable ramp rates, even compared with NGCC, they also result in much higher LCOE, so that their utilization is usually relegated to periods of remarkably high prices and demand [3].

Despite the fact that NGCC power plants emit less GHG compared with other fossil-fuel-based generators, if economic penalties associated with CO₂ emissions are instantiated, which many consider a likely outcome in the near future, it would be difficult to make a case that sees current NGCC power plants overcome these penalties and retain a substantial fraction of the energy generation. However, if proven technologies such as post-combustion carbon capture (PCC) can reduce the CO₂ emitted by NGCC power plants before it enters the atmosphere, making these

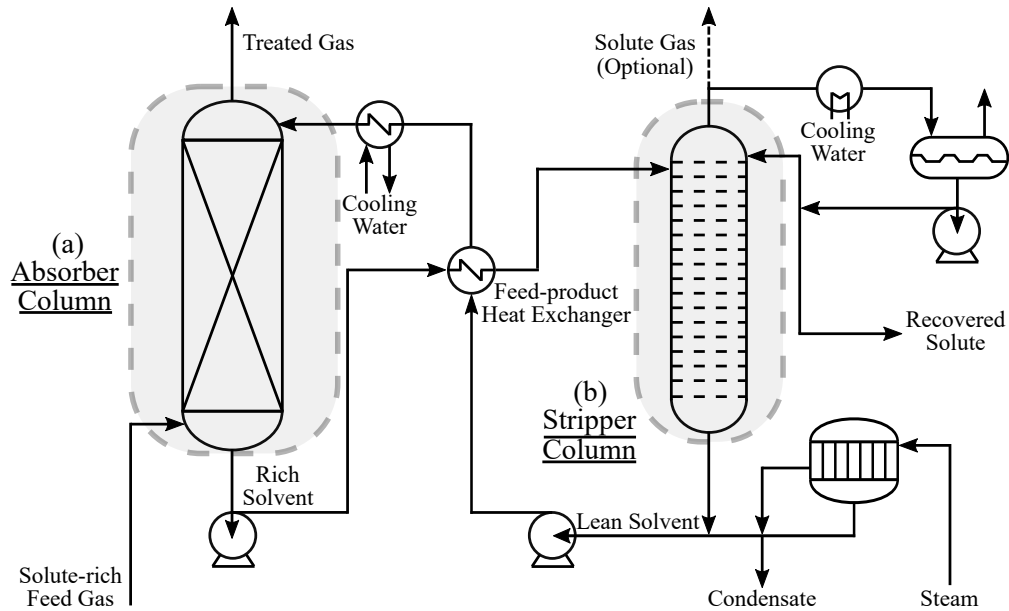


Figure 1.3: Illustration of (a) CO₂ solvent-based absorber and (b) stripper for solvent regeneration [7] used for post combustion CO₂ capture.

integrated plants essentially carbon-neutral, then really the role played by them in the future could be significant, as many claim [7,21,23,26,27].

1.3 Post-Combustion Carbon Capture

The separation of CO₂ from gas mixtures has been pursued in commercial activities involving hydrogen, ammonia, and natural gas purification plants [7]. Due to the increased concerns regarding the climate crisis in recent years, considerable efforts have been taken to develop larger scale carbon capture (CC) technologies to be implemented within the energy sector. CO₂ can be removed directly from the atmosphere – these technologies are referred to as direct air capture (DAC) – or from the exhaust of power plants, also referred to as post-combustion carbon capture (PCC). There are some inherent differences between DAC and PCC which should guide the design approach of the carbon capture system. For instance, the concentration of CO₂ in the atmosphere is much lower than in the exhaust of a power plant: 0.0390 mol% compared with 12 mol%. Additionally, PCC must also overcome challenges associated with a much higher CO₂ flow rate and overall emissions [7].

The traditional approach for PCC is solvent-based absorption [7]. In the absorption process, the power plant exhaust enters the absorption column – Fig. 1.3a – where the CO₂ is separated from the gas and dissolved in the solvent. An additional and crucial component is the stripping column – Fig. 1.3b – where the CO₂ is removed from the rich solvent using condensing steam. A large fraction of the capital investments for PCC systems is represented by the absorber and stripping columns [7,27]. Most of the power requirement (and costs) associated with PCC systems is represented by the thermal power required to generate steam for solvent regeneration, the electrical power associated with compressing the removed CO₂, and the cost of transport and storage of the compressed CO₂ [27, 28]. In the specific case of NGCC power plants, the steam for solvent regeneration is extracted directly from the low-pressure steam turbine, which incurs a 10% power net power decrease [1, 27, 29].

Table 1.2: Parameters comparison between an NGCC power plant with (B31B) and without PCC (B31A).

Parameter	Units	B31A	B31B	Difference %
Capacity Factor	%	85	85	–
Nominal CO ₂ Capture	%	0	90	–
Gross Power Output	MW	740	690	-6.76
Auxiliary Power Requirement	MW	14	44	214.3
Net Power Output	MW	727	746	-11.14
CO ₂ Emissions	lb/MW net	755	85	-88.74
Total Plant Cost	\$/kW	780	1984	154.36
LCOE	\$/MWh	43.3	70.9	63.74

PCC systems have demonstrated that 90+% CO₂ removal rates are achievable [30]. This is encouraging in the light of possible CO₂ penalties discussed in Sec. 1.1. However, as shown in Tab. 1.2, a high CO₂ capture rate comes at the cost of substantial penalties placed on the system: performance penalties in the form of lower flexibility, decreased gross and net power output; economic penalties due to the substantial capital investment necessary for the CC system; and increased operational costs. These factors contribute to an overall increase in LCOE for the NGCC power plant coupled with CC, from 43.3 \$/MWh to 70.9 \$/MWh. For these reasons, despite relatively high CO₂ are feasible, it has been difficult to make a solid commercial case for CC systems

coupled with any fossil fuel-based generators, including NGCC plants [21, 27–32]. However, solutions have been proposed to overcome these limitations and make CC profitable: some include coupling CC with external energy storage [21, 31], storing CO₂-rich solvent to limit CC's parasitic load at peak electricity prices [28, 33], and venting the CO₂ when more profitable than using CC [34]. A slightly different proposed solution consists in integrating NGCC and CC with hot thermal energy storage (HS) and cold thermal energy storage (CS) units [5, 6]. This approach is investigated in more detail in Sec. 1.4.

1.4 Coupling Thermal Energy Storage with Carbon Capture

The existing solutions to increase the flexibility of PP coupled with PCC show limitations that make them unfeasible for scenarios that call for PCC in the first place [6]. For instance, while CO₂ venting allows a reduction in the impact of the CC system's parasitic load onto the host plant, the penalty from emitting CO₂ into the atmosphere in the context of aggressive carbon policies might make this an unfeasible approach [35]. Moreover, storing CO₂ in the solvent itself might seem like an attractive solution as it does offset the parasitic load from the CC system at peak electricity prices. However, for implementing this approach, the size of the equipment for solvent regeneration must be increased (and with it the capital investment), or the CO₂ rate must be decreased [34]. In either case, results have shown that this approach might not be economically feasible in scenarios that justify PCC in the first place [6, 35].

Integrating concrete hot thermal energy storage (HS) and cold thermal energy storage (CS) with NGCC power plants coupled with CC denotes an alternative approach to make PCC economically feasible. As thermal energy storage (TES) units, HS and CS are technologies that have been already investigated in the context of power generation, but never as coupled with PCC [6, 36–39].

The modes of operation of the TES units as coupled with NGCC plants with CC are better understood in reference to Fig. 1.4. In the neutral phase – Fig. 1.4a – similar to the nominal operation of an NGCC plant with CC but not TES, thermal energy is extracted from the NGCC itself to provide the steam necessary to the CC for solvent regeneration; additional electrical loads

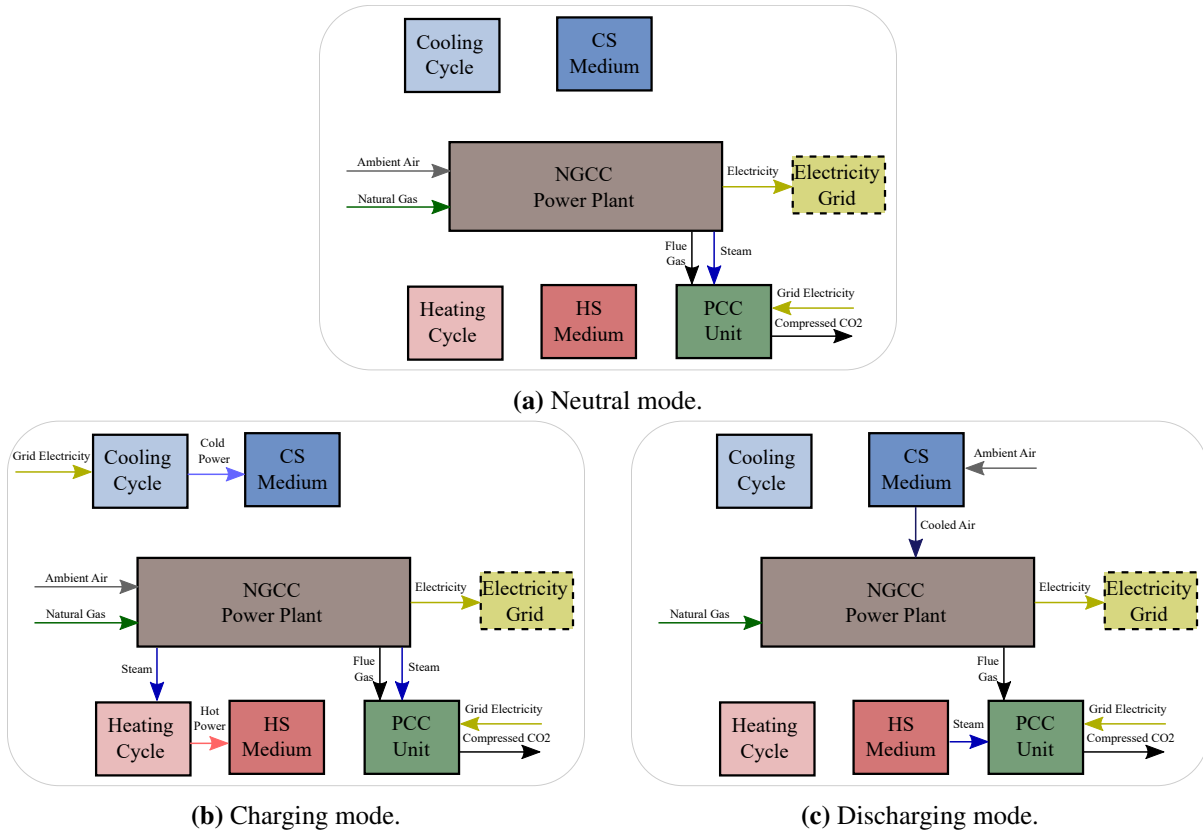


Figure 1.4: Simplified diagram of the different operation modes of TES units coupled with an NGCC plant and PCC [5].

to power mainly the CO₂ compressors also penalize the net power output of the system. In the charging phase – Fig. 1.4b – hot thermal energy is generated in the HS by extracting it from the PP; whereas cold thermal energy is generated in the CS through a vapor compression cycle powered by grid electricity. Note that in this example, the HS requires the PP to be online in order to be charged. However, HS configurations have been studied which also use grid electricity to charge (i.e., using resistive heating), so that charging of both HS and CS can occur with the PP being offline [5, 6]. In the discharging mode in Fig. 1.4c, the CC is still running at nominal capacity, but the steam required for solvent regeneration is now extracted from the HS, reducing the net penalty suffered by the NGCC plant. In addition, the discharging of the CS actively cools the air entering the NGCC combustion chamber, increasing its density and thus the amount of fuel that can be combusted. Therefore the power generated by the NGCC is beyond its nominal value [5, 6]. Moreover, an additional operational phase that is not shown in Fig. 1.4 is the so-

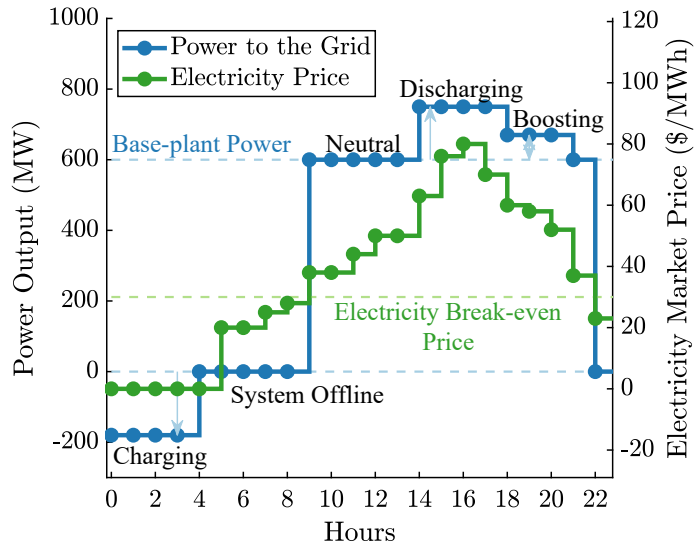


Figure 1.5: Simplified operation of the TES in response to variable electricity prices.

called “boosting mode” and essentially consists in simultaneously charging and discharging the CS without operating the HS. Since the round-trip efficiency of the CS can be larger than unity (i.e., the net increase in power output from discharging the CS is larger than the penalty from charging it), the boosting mode allows for a resulting slight increase in net power output of the NGCC power plant, at the cost of increased fuel consumption and decreasing the percentage of CO₂ captured [6].

The operational modes described in Fig. 1.4 grant additional flexibility to the NGCC power plant equipped with CC and provide opportunities for increased profit in response to variable electricity prices. Fig. 1.5 shows an illustration of how the different operational modes might be utilized during a given time 24-hr time interval. From 0-hr to 8-hr, the electricity prices are near 0 \$/MWh, so it is not profitable to run the NGCC. However, such low prices are suitable for charging the TES units if that is done using electricity: this results in negative PP from 0-hr to 4-hr, which signals that electricity is being extracted from the grid to charge the TES units until at full capacity. From 9-hr to 13-hr, while the electricity prices increase above the break-even line of the PP, the NGCC plant turns on in the neutral mode, as in Fig. 1.4a. The electricity prices peak between 14-hr to 17-hr, so that in this time interval there is potential for a large profit, which is captured by operating

Table 1.3: Several TES configurations and their working principles, as presented in [5, 6].

#	Heat Pump Type	Energy Source	Working Fluid
1 [†]	Brayton Cycle	Flue Gas	Flue Gas
2 [†]	Brayton Cycle	Electricity	Ambient Air
3 [†]	Brayton Cycle	Flue Gas	Ambient Air
4	Vapor Compression	Flue Gas	Ambient Air
5	Vapor Compression	Flue Gas	Steam
6 [†]	Tiered Vapor Compression	Electricity	Steam, Ammonia, Coolant
7	LP Steam Turbine	Direct Extraction	Steam
8	IPT Steam Turbine	Direct Extraction	Steam
9	Resistive Heating	Electricity	Air
10 [*]	Vapor Compression	Electricity	Ammonia

[†] combines HS and CS in one configuration

^{*} CS configuration

the NGCC at full capacity and discharging the HS and CS, allowing for an increased PP while still capturing CO₂ through the CC. From 18-hr to 20-hr, the electricity prices are still relatively high, but the TES units have been emptied: higher-than-nominal power output is achieved through the boosting mode. Finally, as the prices start dropping, the system cycles back to the neutral mode before going offline and waiting for the next cycle. An important detail is that despite Figs. 1.4 and 1.5 showing the HS and CS as consistently operating in identical modes, they can be fundamentally separated technologies which are independent in their operation (and in their design). However, their most effective operations follow similar motivations, so their respective operational modes do often tend to align.

Figure 1.4 shows a high-level description of the HS and CS units in the main operation modes for non-specific technologies. To generate the hot and cold thermal energy necessary to charge the TES units, numerous thermodynamics cycles, working fluids, and technical equipment might be used. In work based on the optimization model in this thesis, a total of 17 different thermal energy storage configurations have been evaluated [5, 6]. Table 1.3 presents a high-level description of the most relevant configurations, highlighting the type of heat pump and the working fluid used.

TES constitutes a promising technology in order to make CC coupled with NGCC power plants more profitable: its implementation would retain the output flexibility of NGCC power plants while allowing CC to operate at steady-state. Also, it would derestrict the NGCC plant beyond nominal

operation output during peak price periods by utilizing stored energy from the TES for solvent regeneration and air pre-chilling. Understanding how the different operational parameters of the TES configurations presented in Tab. 1.3 translate into economic performance in real and future energy markets is crucial for selecting and further improving the most promising technology: Chap. 2.1 will present how a fair comparison can be achieved, and Sec. 3.5 will discuss some results. More details on the technology modeling of the TES units are available in [5, 6]. Finally, for the HS and CS media, concrete blocks have been selected for storing and realizing thermal energy. This choice was guided by their relatively low cost, remarkable durability, and flexibility to accommodate large temperature swings [6].

1.5 Control Co-design Optimization

The questions associated with the early-stage design and the economic evaluation of a system such as an NGCC power plant with CC and TES call for a computational model which integrates plant design decisions as well as control decisions that must dynamically respond to time-varying signals such as electricity and fuel prices, CO₂ taxes, and temperature data. The strategy underlying this work represents the system within a control co-design (CCD) optimization problem. As a growing class of integrated design techniques, CCD considers plant design and control decisions in an integrated manner and has shown significant advantages in solving complex design problems over traditional sequential and siloed approaches [40, 41].

There are two fundamental coordination strategies for posing a CCD problem: 1) a simultaneous problem formulation, in which both plant design and control optimization variables are considered within a single optimization problem; 2) a nested formulation, in which two optimization problems are formulated: the outer-loop problem, in which usually only plant design variables are considered optimization variables, and the inner-loop control subproblem, where the design of the plant is fixed, and the control of the plant is optimized [8, 40]. Towards formalizing this

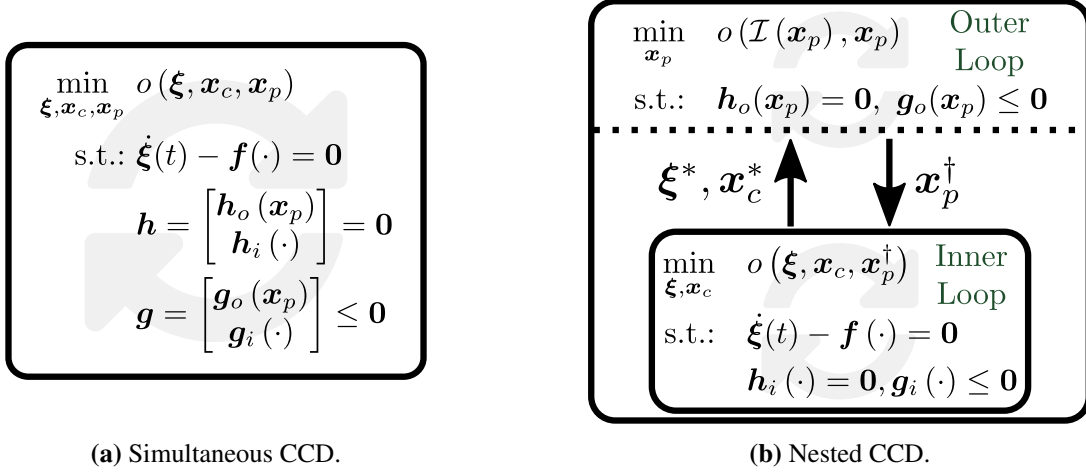


Figure 1.6: Illustration of the two fundamental CCD strategies [8].

strategy, Eq. (1.1) shows a general CCD optimization problem, expressed in a simultaneous form:

$$\underset{x=[\xi, x_c, x_p]}{\text{minimize:}} \quad o = m(\xi_0, \xi_f, x_c, x_p) + \int_{t_0}^{t_f} \ell(t, \xi, x_c, x_p) dt \quad (1.1a)$$

$$\text{subject to:} \quad \dot{\xi}(t) - f(t, \xi, x_c, x_p) = 0 \quad (1.1b)$$

$$h = \begin{bmatrix} h_o(x_p) \\ h_i(t, \xi, x_c, x_p, \xi_0, \xi_f) \end{bmatrix} = 0 \quad (1.1c)$$

$$g = \begin{bmatrix} g_o(x_p) \\ g_i(t, \xi, x_c, x_p, \xi_0, \xi_f) \end{bmatrix} \leq 0 \quad (1.1d)$$

$$\text{where:} \quad \xi_0 = \xi(t_0), \quad \xi_f = \xi(t_f) \quad (1.1e)$$

where (ξ, x_c, x_p) are respectively the state, plant control and design optimization variables; $o(\cdot)$ is the objective function of the problem, and is composed by the Lagrange term $\ell(\cdot)$ which is integrated between $t \in [t_0, t_f]$, and the Mayer term $m(\cdot)$, which is time-independent. The dynamic constraints of the state variables $\xi(t)$ are represented by the first-order differential equation in Eq. (1.1b); Equation (1.1c) represents the equality constraints of the problem, which are divided into two distinct sets $\{h_o(\cdot), h_i(\cdot)\}$, where $h_o(\cdot)$ depends only on the plant design variables x_p . A similar partitioned form is used for the inequality constraints $g(\cdot)$ [42].

Figure 1.6 shows a high-level comparison of simultaneous and nested CCD coordination strategies based on the problem in Eq. (1.1). There are advantages and disadvantages associated with each of these coordination strategies [8,40], with the appropriate choice depending on the specifications of the problem at hand. In the context of this work, both coordination strategies are explored and implemented: the simultaneous formulation is more computationally efficient and allows for the evaluation of the TES technology assuming perfect foresight of the scenario’s techno-economic signals, whereas the nested approach is used when a more realistic control strategy is implemented (which assumes only limited knowledge of future signals – see Sec. 2.2.3).

1.6 Research Questions

Although a promising concept, the complexities of an NGCC power plant coupled with CC, HS, and CS pose certain design and control challenges, including the following decisions that are addressed in this thesis:

1. For profitable implementation, each of the aforementioned subsystems (NGCC, CC, HS, CS) needs to simultaneously operate in response to time-varying external signals such as electricity and fuel price, CO₂ tax, and ambient temperature.
2. Sizing decisions accompanying the physical realization of such subsystems are strictly dependent on their day-to-day operation. These decisions include, for example, selecting the appropriate storage capacity for the respective TES units, as well as the charging and discharging power capacity. Usually, design decisions of this kind speak to trade-offs between the performance achievable by a system and the capital investments required to attain it. It is crucial to thoroughly investigate these trade-offs to achieve the best economic performance of the system and provide a fair comparison against the state-of-the-art.
3. At a fundamental level, as mentioned in Sec. 1.4, because of the novelty surrounding TES technologies as applied to NGCC power plants with CC, many fundamental questions need to be answered regarding the appropriate equipment to be used for generating or extracting

thermal power for charging the TES units, as well as for discharging them. Therefore, while the parameters describing the different TES configurations can be generated from individual and detailed thermodynamics analysis, the architecture of the model needs to be configurable to allow for the efficient evaluation of TES technologies with different characteristics and operational constraints while still accurately representing their dynamics with a high time resolution.

4. An authentic evaluation of the system as a whole needs to reflect operation as close to real-world conditions as possible. For instance, considerations related to the impact of location and ambient temperature on the performance of the system should be included, and limitations on the information foresight on provided market and environmental signals must be studied.
5. Many large-scale studies might need to be conducted to explore various TES technologies against a significant number of different technical, economic, and geographical assumptions. Therefore, the implementation of the model as a computer program needs to be efficient to allow for these studies to take place.

1.7 Summary and Thesis Content

Based on the previous discussion, investigating a TES system coupled with NGCC power plants and CC in broader consideration about the expected evolution of energy markets, the motivations underlying the need for a flexible and efficient computational model for a realistic economically-driven evaluation of this novel technology were introduced. The rest of this document provides a detailed description of the optimization model and is organized as follows: Chap. 2.1 reports the derivation and the formulation of the optimization problem at the base of this approach; Chap. 3 presents the results of several different case studies demonstrating the capabilities of the optimization model to make sound economic judgments of the proposed system. Finally, Chap. 4 presents the main conclusions from this analysis as well as some recommendations for future work.

Chapter 2

Optimization Problem Formulation and Strategy

Based on the research questions presented in Sec. 1.6 underlying the early-stage modeling and economic feasibility assessment of TES technology as coupled with NGCC power plants and CC, this chapter presents the thorough derivation of an optimization-based mathematical model tailored to the maximization of the net present value (NPV) of this system. Based on the discussion in Sec. 1.5, the model is first posed as a continuous simultaneous CCD problem in Sec. 2.1, while Sec. 2.2 discusses additional details about the model and strategies regarding obtaining solutions.

2.1 Problem Formulation

In this section, the dynamic optimization model of an NGCC power plant, coupled with CC, HS, and CS units as well as the NPV calculation are presented. Because of the dynamic nature of the model, many of the problem variables depend on time t . In addition, some of the model variables also depend on ambient temperature T_0 , which is provided to the model as a time-dependent signal $T_0(t)$. Figure 2.1 is a high-level representation of each of the subsystems and the energy flows between them. Different arrow colors in the image represent different forms or power, including heat transfer, electrical power, and inlet-cooling power from discharging the CS (which increases the efficiency and capacity of the PP). Many of the specific parameters used in the case study are in App. A.

2.1.1 Thermal Energy Storage

Plant Variables and Constraints

There are three plant variables associated with each of the TES units:

$$p = \left[\Sigma_{\text{HS}} \quad P_{\text{HS},\text{in}} \quad P_{\text{HS},\text{out}} \quad \Sigma_{\text{CS}} \quad P_{\text{CS},\text{in}} \quad P_{\text{CS},\text{out}} \right]^T \quad (2.1)$$

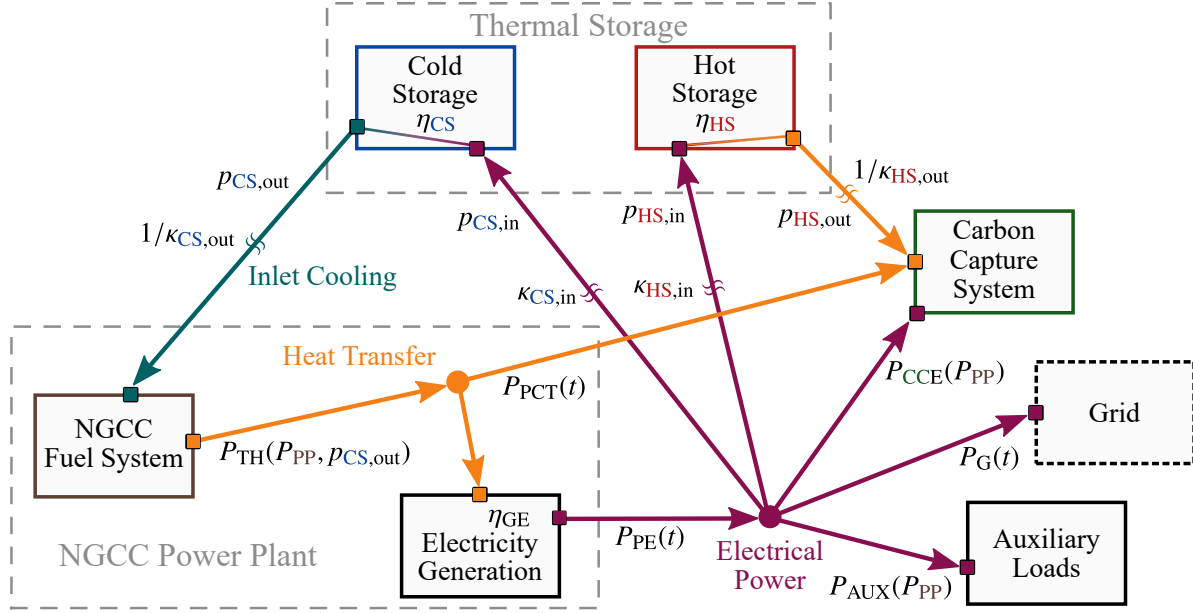


Figure 2.1: Key subsystems and the flows between them.

where $(\Sigma_{HS}, P_{HS,in}, P_{HS,out})$ are the HS storage capacity, maximum energy transfer rate into the HS, and maximum energy transfer rate out of the HS, respectively, and $(\Sigma_{CS}, P_{CS,in}, P_{CS,out})$ are the equivalent plant variables for the CS.

To ensure that the hot and cold TES capacities are non-negative, we impose the following constraints:

$$\Sigma_{HS} \geq 0 \quad \Sigma_{CS} \geq 0 \quad (2.2)$$

where no thermal storage is an option if the lower bound is active.

Since the HS configuration's purpose to take over the CC reboiler duty, we assume that the maximum energy rate from the HS is the provided nominal design; to avoid technical limitations, we make a similar assumption for the CS. In addition, we enforce the energy rate from the TES units to be non-negative. These points are summarized with the following constraints:

$$0 \leq P_{HS,out} \leq \bar{P}_{HS,out} \quad 0 \leq P_{CS,out} \leq \bar{P}_{CS,out} \quad (2.3)$$

Similarly, there are technical limitations imposed onto the maximum charging rates, as well as non-negativity:

$$0 \leq P_{\text{HS},\text{in}} \leq \bar{P}_{\text{HS},\text{in}} \quad 0 \leq P_{\text{CS},\text{in}} \leq \bar{P}_{\text{CS},\text{in}} \quad (2.4)$$

Control Variables and Constraints

As TES units, both the **HS** and **CS** can dynamically store and release thermal power; these are the four control variables:

$$\mathbf{u}_T(t) = \left[p_{\text{HS},\text{in}}(t) \quad p_{\text{HS},\text{out}}(t) \quad p_{\text{CS},\text{in}}(t) \quad p_{\text{CS},\text{out}}(t) \right]^T \quad (2.5)$$

where $(p_{\text{HS},\text{in}}, p_{\text{CS},\text{in}})$ are the equivalent input power to the **HS** and the **CS** from the electricity generator, respectively; $p_{\text{HS},\text{out}}$ is the output power from the **HS** to the **CC**; and $p_{\text{CS},\text{out}}$ is the output power from the **CS** to the **PP** module.

To ensure that the non-negative power inputs are less than the limits, we include the following inequality constraints:

$$0 \leq p_{\text{HS},\text{in}}(t) \leq \mu_{\text{HS},\text{in}}(T_0) \cdot P_{\text{HS},\text{in}} \quad (2.6a)$$

$$0 \leq p_{\text{CS},\text{in}}(t) \leq \mu_{\text{CS},\text{in}}(T_0) \cdot P_{\text{CS},\text{in}} \quad (2.6b)$$

where $(\mu_{\text{HS},\text{in}}, \mu_{\text{CS},\text{in}})$ define the fraction of the nominal power input available at the current temperature T_0 . Similar constraints are imposed on the allowed power outputted from the TES units:

$$0 \leq p_{\text{HS},\text{out}}(t) \leq \mu_{\text{HS},\text{out}}(T_0) \cdot P_{\text{HS},\text{out}} \quad (2.7a)$$

$$0 \leq p_{\text{CS},\text{out}}(t) \leq \mu_{\text{CS},\text{out}}(T_0) \cdot P_{\text{CS},\text{out}} \quad (2.7b)$$

where $(\mu_{\text{HS},\text{out}}, \mu_{\text{CS},\text{out}})$ similarly constraint the effective discharging power available to the TES units at any time.

States and Constraints

There are two key state for the TES units, namely the current amount of stored thermal energy, (E_{HS} , E_{CS}) respectively. The differential equations are simple balances between the input and output powers for each:

$$\dot{E}_{\text{HS}} = \kappa_{\text{HS},\text{in}} \cdot p_{\text{HS},\text{in}}(t) - \kappa_{\text{HS},\text{out}} \cdot p_{\text{HS},\text{out}}(t) \quad (2.8a)$$

$$\dot{E}_{\text{CS}} = \kappa_{\text{CS},\text{in}} \cdot p_{\text{CS},\text{in}}(t) - \kappa_{\text{CS},\text{out}} \cdot p_{\text{CS},\text{out}}(t) \quad (2.8b)$$

where ($\kappa_{\text{HS},\text{in}}$, $\kappa_{\text{CS},\text{in}}$) are the coefficients converting the electricity subtracted from the PP to thermal power to the TES units; whereas ($\kappa_{\text{HS},\text{out}}$, $\kappa_{\text{CS},\text{out}}$) indicate the conversion from the TES discharging electrical power to the thermal power flowing out of the TES units. The initial states of the thermal storage subsystems are:

$$E_{\text{HS}}(t_0) = E_{\text{HS},0} \quad E_{\text{CS}}(t_0) = E_{\text{CS},0} \quad (2.9)$$

To ensure that the thermal energy storage is positive and below the maximum level allowed, we finally include:

$$0 \leq E_{\text{HS}}(t) \leq \Sigma_{\text{HS}} \quad 0 \leq E_{\text{CS}}(t) \leq \Sigma_{\text{CS}} \quad (2.10)$$

2.1.2 Natural Gas Combined Cycle Power Plant

Control Variables and Constraints

There is one control optimization variable associated with the NGCC power plant, which represents the requested power output:

$$\mathbf{u}_p(t) = \left[p_{\text{PP}}(t) \right]^T \quad (2.11)$$

We include a constraint to ensure the requested power output to be non-negative and less than the allowed limits:

$$0 \leq p_{PP}(t) \leq \mu_{PP}(T_0) \cdot \bar{P}_{PP} \quad (2.12)$$

where \bar{P}_{PP} is the provided maximum nominal power of the NGCC and μ_{PP} defines the fraction of power available depending on the ambient temperature.

States and Constraints

The requested power output in Eq. (2.11) is used in a dynamic equation describing the PP power level P_{PP} , a state variable in the problem:

$$\dot{P}_{PP}(t) = \frac{1}{\tau_{PP}} \left(-P_{PP}(t) + p_{PP}(t) \right) \quad (2.13)$$

where (τ_{PP}) is the ramp rate of the PP. The initial state of the PP is:

$$P_{PP}(t_0) = P_{PP,0} \quad (2.14)$$

We also include a constraint to ensure the effective power output to be non-negative and less than the allowed limits:

$$0 \leq P_{PP}(t) \leq \mu_{PP}(T_0) \cdot \bar{P}_{PP} \quad (2.15)$$

where \bar{P}_{PP} is the provided upper bound on the NGCC power output.

During combined operation of the PP and TES, we would like to limit charging and discharging of TES to only when the PP is operating, so we include the following inequality constraints:

$$p_{HS,in}(t) \leq P_{PP}(t) \quad p_{CS,in}(t) \leq P_{PP}(t) \quad (2.16a)$$

$$p_{HS,out}(t) \leq P_{PP}(t) \quad p_{CS,out}(t) \leq P_{PP}(t) \quad (2.16b)$$

so energy can only flow to or from any TES element if $P_{PP} > 0$.

Intermediate Functions

From a combination of plant and control variables, states, and problem parameters from the HS, CS, and PP, the instantaneous fuel consumption of the PP is:

$$m_f(t) = \rho_f \cdot \mu_f \cdot P_{PP}(t) + \Delta\rho_f \cdot \mu_{\Delta f}(T_0) \cdot p_{CS,out}(t) \quad (2.17)$$

where ρ_f is the nominal conversion factor between power output generated by the NGCC and fuel consumed, and $\Delta\rho_f$ is the same quantity but associated with discharging the CS. $(\mu_f, \mu_{\Delta f})$ are factors affecting these quantities depending on the ambient temperature. Equation (2.17) represents a fundamental intermediate function in the calculation of the expenses associated with running the system in Eq. (2.28b).

2.1.3 Carbon Capture

The CC subsystem is implemented such that it is always operating when the PP is operating. Therefore, all its characteristics are dependent on the signals described in the previous subsection. One of the key aspects of the CC subsystem is the instantaneous CO₂ capture rate, which is:

$$\beta_C(t) = c_n \cdot \mu_c(T_0) \cdot P_{PP}(t) - \Delta c_d \cdot \mu_{\Delta c}(T_0) \cdot p_{CS,out}(t) \quad (2.18)$$

where c_n is the percentage of carbon captured from the flue gas when the PP runs in the neutral state, and Δc_d is the decrease in capture when the CS is being discharged. $(\mu_c, \mu_{\Delta c})$ describe how these nominal capture rates are affected by ambient temperature. Here, we are assuming that total amount of CO₂ generated by the whole system is directly proportional to the fuel burned, m_f from Eq. (2.17), according to the conversion coefficient α_C . It follows that of the total CO₂ generated,

the portion captured and emitted into the atmosphere are respectively:

$$m_{C,\text{in}}(t) = m_f(t) \cdot \alpha_C \cdot \beta_C(t) \quad (2.19a)$$

$$m_{C,\text{out}}(t) = m_f(t) \cdot \alpha_C \cdot (1 - \beta_C(t)) \quad (2.19b)$$

As currently described, $(m_{C,\text{in}}, m_{C,\text{out}})$ are nonlinear terms in the objective function. We have found that we can maintain the linearity without virtually losing any accuracy in the solution by approximating the expressions above using two known points of operation: 1) the neutral phase of the PP, and 2) the discharging phase of the CS. So we rewrite Eq. (2.19) as:

$$\hat{m}_{C,\text{in}}(t) = \underline{\rho}_{C,\text{in}}(T_0) \cdot P_{\text{PP}}(t) + \Delta\rho_{C,\text{in}}(T_0) \cdot p_{\text{CS},\text{out}}(t) \quad (2.20a)$$

$$\hat{m}_{C,\text{out}}(t) = \underline{\rho}_{C,\text{out}}(T_0) \cdot P_{\text{PP}}(t) + \Delta\rho_{C,\text{out}}(T_0) \cdot p_{\text{CS},\text{out}}(t) \quad (2.20b)$$

where $(\underline{\rho}_{C,\text{in}}, \underline{\rho}_{C,\text{out}})$ are the CO₂ captured and emitted by the whole system in neutral mode per unit power generated:

$$\underline{\rho}_{C,\text{in}} = \alpha_C \cdot \rho_f \cdot \mu_f(T_0) \cdot c_n \cdot \mu_c(T_0) \quad (2.21a)$$

$$\underline{\rho}_{C,\text{out}} = \alpha_C \cdot \rho_f \cdot \mu_f(T_0) \cdot (1 - c_n \cdot \mu_c(T_0)) \quad (2.21b)$$

and $(\Delta\rho_{C,\text{in}}, \Delta\rho_{C,\text{out}})$ are the coefficients describing the linear trajectory from the neutral phase to the maximum discharging of the CS, per unit power generated from discharging the CS. There are thermal and electrical power requirements, respectively P_{CCT} and P_{CCE} , to run the CC unit, which depend on the technology implemented, the PP power level, and the nominal CO₂ capture percentage $\bar{\beta}_C$:

$$P_{\text{CCT}} = P_{\text{CCT}}(P_{\text{PP}}, \bar{\beta}_C) \quad P_{\text{CCE}} = P_{\text{CCE}}(P_{\text{PP}}, \bar{\beta}_C) \quad (2.22)$$

where P_{CCE} is electrical power directly extracted from the PP output, while P_{CCT} is thermal power in the form of steam, which is either also extracted from the PP or is provided by discharging the HS. It follows that the power that must be extracted from the PP is whatever fraction of P_{CCT} that is not provided by the HS:

$$P_{\text{PCT}}(t) = P_{\text{CCT}}(P_{\text{PP}}, \bar{\beta}_{\text{C}}) - \eta_{\text{HS}} \cdot p_{\text{HS, out}}(t) \quad (2.23)$$

where η_{HS} accounts for any efficiency losses.

2.1.4 Electricity Generation

The electricity generated by the system is the primary source of revenue driving the NPV objective. The corrected thermal power outputted from the PP, here indicated as P_{TH} , depends on the PP level and on the discharging of the CS:

$$P_{\text{TH}}(t) = P_{\text{PP}}(t) + \eta_{\text{CS}} \cdot p_{\text{CS, out}}(t) \quad (2.24)$$

where η_{CS} represents any efficiency losses from discharging the CS. The gross electricity generated is then:

$$P_{\text{PE}}(t) = \eta_{\text{GE}} \cdot (P_{\text{TH}}(t) - P_{\text{PCT}}(t)) \quad (2.25)$$

where η_{GE} is the efficiency of conversion between thermal and electrical power, and P_{PCT} is the thermal power diverted to the CC as in Eq. (2.23). From the gross electrical power generated by the system, a fraction is diverted to the CC in Eq. (2.22); a fraction might be sent to charge the TES units; finally, some power is required to satisfy the system's auxiliary loads P_{AUX} , which can depend on the state of the PP. Therefore, the net power outputted to the grid is:

$$P_{\text{G}} = P_{\text{PE}} - P_{\text{CCE}} - p_{\text{HS, in}} - p_{\text{CS, in}} - P_{\text{AUX}} \quad (2.26)$$

2.1.5 Techno-Economic Analysis

Revenue and Expenses

v_{rev} is the revenue gained by outputting power to the grid P_G calculated in Eq. (2.26) at the current electricity price c_{elec} :

$$v_{\text{rev}}(t) = c_{\text{elec}}(t) \cdot P_G(t) \quad (2.27)$$

and v_{exp} represents the expenses of the system, which are divided in cost of fuel v_{fuel} and other operation costs v_{op} :

$$v_{\text{exp}}(t) = v_{\text{fuel}}(t) + v_{\text{op}}(t) \quad (2.28a)$$

$$v_{\text{fuel}}(t) = c_{\text{fuel}}(t) \cdot m_f(t) \quad (2.28b)$$

$$v_{\text{op}}(t) = c_{\text{CO}_2} \cdot \hat{m}_{\text{C,out}}(t) + C_{\text{VOM}}(t) + C_{\text{FOM}}(t) \quad (2.28c)$$

where $(m_f, \hat{m}_{\text{C,out}})$ are the instantaneous fuel consumed and CO_2 emitted into the atmosphere by the system, respectively, as described in Eqs. (2.17) and (2.20b). Conversely, c_{fuel} is the instantaneous fuel market price, while c_{CO_2} is the selected carbon tax. C_{VOM} encompasses all the additional costs which directly depend on the active utilization of each of the subsystems:

$$\begin{aligned} C_{\text{VOM}}(t) = & c_{\text{PP,VOM}} \cdot P_{\text{PP}}(t) + c_{\text{CC,VOM}} \cdot \hat{m}_{\text{CO}_2,\text{in}}(t) + c_{\text{HS,VOM}} \cdot (p_{\text{HS,in}}(t) + p_{\text{HS,out}}(t)) \cdots \\ & + c_{\text{CS,VOM}} \cdot (p_{\text{CS,in}}(t) + p_{\text{CS,out}}(t)) \end{aligned} \quad (2.29)$$

where the first term depends on the PP power level P_{PP} ; the second term depends on the CO_2 captured by the system from Eq. (2.20a); the last two terms are associated with the power charging and discharged by both TES units. Finally, C_{FOM} includes the fixed operation costs from each of

the subsystems, which are independent from their utilization:

$$C_{\text{FOM}}(t) = c_{\text{PP,FOM}} + c_{\text{CC,FOM}} + c_{\text{HS,FOM}} \cdot (P_{\text{HS,in}} + P_{\text{HS,out}}) \cdots \\ + c_{\text{CS,FOM}} \cdot (P_{\text{CS,in}} + P_{\text{CS,out}}) + c_{\text{HS,TES,FOM}} \cdot \Sigma_{\text{HS}} + c_{\text{CS,TES,FOM}} \cdot \Sigma_{\text{CS}} \quad (2.30)$$

Capital Costs

The system's capital costs C_{cap} are:

$$C_{\text{cap}}(\mathbf{p}) = C_{\text{PP}} + C_{\text{CC}} + C_{\text{HS}}(\mathbf{p}) + C_{\text{CS}}(\mathbf{p}) \quad (2.31)$$

where $(C_{\text{PP}}, C_{\text{CC}})$ are the fixed capital investment to realize the PP and the CC subsystems, while $(C_{\text{HS}}, C_{\text{CS}})$ are the costs for the TES units and depend on \mathbf{p} :

$$C_{\text{HS}}(\mathbf{p}) = c_{\text{HS,in}} \cdot P_{\text{HS,in}} + c_{\text{HS,out}} \cdot P_{\text{HS,out}} + c_{\text{HS,TES}} \cdot \Sigma_{\text{HS}} \quad (2.32a)$$

$$C_{\text{CS}}(\mathbf{p}) = c_{\text{CS,in}} \cdot P_{\text{CS,in}} + c_{\text{CS,out}} \cdot P_{\text{CS,out}} + c_{\text{CS,TES}} \cdot \Sigma_{\text{CS}} \quad (2.32b)$$

where $(c_{\text{HS,in}}, c_{\text{HS,out}})$ represent the capital costs scaling with the desired charging and discharging power capacity of the HS unit, while $c_{\text{HS,TES}}$ is the cost of the HS medium. Conversely, $(c_{\text{CS,in}}, c_{\text{CS,out}}, c_{\text{CS,TES}})$ represent the similar costs for the CS. The following subsection analyzes more in depth the economic model for calculating the net present value of the overall system, the primary metric of interest.

Net Present Value Calculation

NPV was selected as main economic indicator for the proposed system, because it represents the return on investment over its entire lifetime [43]. Other indicators, such as LCOE, are typically used for power generation systems, but due to the arbitrage nature of the system being evaluated, they would not accurately represent its benefit.

In simplified terms, NPV is the difference between the present value of cash inflows and the present value of cash outflows during a period of time. To convert future values into a present value, a discount factor DF is used, which depends on the year evaluated y and the selected rate of return IRR :

$$DF(y) = \frac{1}{(1 + IRR)^y} \quad (2.33)$$

Assuming the capital investment to build the plant is made before the start of the operation, an equation to calculate NPV is:

$$NPV = V_{\text{income}} - C_{\text{cap}} \quad (2.34)$$

The income generated from the system V_{income} is the summation of the profit made discounted over the system's lifetime, here represented by the loan term L_t and expressed in units of years y :

$$V_{\text{income}} = \sum_{y=1}^{L_t} (V_{\text{rev}}(y) - V_{\text{exp}}(y)) \cdot DF(y) \quad (2.35)$$

where $(V_{\text{rev}}, V_{\text{exp}})$ are respectively the revenue and expenses from running the system, which are based on Eq. (2.27) and (2.28a) and are obtained upon integration over a year of operation:

$$V_{\text{rev}}(y) = \int_0^{T_{\text{year}}} [v_{\text{rev}}(t) \cdot (1 + i_e)^{y-1}] dt \quad (2.36a)$$

$$V_{\text{exp}}(y) = \int_0^{T_{\text{year}}} [v_{\text{fuel}}(t) \cdot (1 + i_f)^{y-1} + v_{\text{op}}(t)] dt \quad (2.36b)$$

To reduce the size of the problem, in this analysis we assume the control strategy of the plant over its lifetime is identical to that of the first year of operation ($t \in [0, T_{\text{year}}]$). However, we reflect the expected annual increase in electricity and fuel prices with the factors (i_e, i_f) . We use Eq. (2.36)

to rewrite V_{income} as:

$$V_{\text{income}} = \int_0^{T_{\text{year}}} \sum_{y=1}^{L_t} \begin{bmatrix} v_{\text{rev}}(t) & -v_{\text{fuel}}(t) & -v_{\text{op}}(t) \end{bmatrix} \begin{bmatrix} r_e^{y-1} \\ r_f^{y-1} \\ r_d^{y-1} \end{bmatrix} dt \quad (2.37)$$

where: $r_e = \frac{1 + i_e}{1 + IRR}$ $r_f = \frac{1 + i_f}{1 + IRR}$ $r_d = \frac{1}{1 + IRR}$

The non-constant terms within the sum in Eq. (2.37) resemble a geometric series for which a closed-form solution exists [44]:

$$\sum_{i=1}^n aq^{i-1} = \frac{a(1 - q^n)}{1 - q} \quad (2.38)$$

Applying the geometric series solution to Eq. (2.37) – the terms which depend on the variable i are substituted by those which depend on y – allows to rewrite the NPV of the system in a more elegant, simpler to evaluate closed form:

$$NPV = -C_{\text{cap}} + \int_0^{T_{\text{year}}} \begin{bmatrix} v_{\text{rev}}(t) & -v_{\text{fuel}}(t) & -v_{\text{op}}(t) \end{bmatrix} \begin{bmatrix} R_e \\ R_f \\ R_d \end{bmatrix} dt \quad (2.39)$$

where: $R_e = \frac{1 - r_e^{L_t}}{1 - r_e}$ $R_f = \frac{1 - r_f^{L_t}}{1 - r_f}$ $R_d = \frac{1 - r_d^{L_t}}{1 - r_d}$

2.1.6 Objective Function and Summary

We now provide a brief summary of the CCD problem described in the previous sections. We start by reporting the six total plant design optimization variables first presented in Eq. (2.1):

$$\mathbf{p} = \left[\Sigma_{\text{HS}} \quad P_{\text{HS,in}} \quad P_{\text{HS,out}} \quad \Sigma_{\text{CS}} \quad P_{\text{CS,in}} \quad P_{\text{CS,out}} \right]^T \quad (2.40)$$

Additionally, there are four control variables associated with operating the TES units defined in Eq. (2.5), and one control variable for the NGCC from Eq. (2.11). Therefore, there is a total of five open-loop controls optimized in the problem:

$$\mathbf{u}(t) = \left[p_{\text{HS,in}}(t) \quad p_{\text{HS,out}}(t) \quad p_{\text{CS,in}}(t) \quad p_{\text{CS,out}}(t) \quad p_{\text{PP}}(t) \right]^T \quad (2.41)$$

Finally, there are three state variables:

$$\boldsymbol{\xi}(t) = \left[E_{\text{HS}}(t) \quad E_{\text{CS}}(t) \quad P_{\text{PP}}(t) \right]^T \quad (2.42)$$

which respectively describe the HS, CS, and PP levels, and whose linear time-invariant (LTI) dynamic equations are shown in Eqs. (2.8) and (2.13). Additionally, there are several inequality and equality constraints (both path and boundary types), but all are linear. Finally, the linear objective function of the problem is to maximize NPV of the system in Eq. (2.39). The unconstrained objective function is:

$$\underset{u, \xi, p}{\text{maximize}} \quad NPV(t, T_0, \mathbf{u}, \boldsymbol{\xi}, \mathbf{p}) \quad (2.43)$$

Overall, the problem is a linear dynamic optimization problem; all constraints are linear and, due to the approximation described in Sec. 2.1.3, the objective is linear as well. Such problems can be efficiently solved using linear solvers [45]. So, much of the complexity in solving this particular CCD problem comes from the complexity of a variety of intermediate functions, combined with a multitude of time-varying environmental inputs and large timescales (and resulting large optimization problem) to consider.

2.2 Optimization Strategy Considerations

Here we discuss additional aspects surrounding the construction and solving of the linear CCD optimization problem from the previous section.

2.2.1 Approximations

One approximation was already discussed in Sec. 2.1.3 where a quadratic expression was linearized to maintain a linear objective function. The maximum error in calculating the NPV found by comparing the exact and linearization results over many real scenarios was never found to be larger than 0.01%. While a quadratic objective function would still result in a linear-quadratic dynamic optimization problem, it was determined that the relatively small error and efficiency of the approximation was worth its implementation.

2.2.2 Problem Discretization

To solve the dynamic optimization posed in Sec. 2.1, direct transcription (DT) is used [45–47]. In this case, the resulting finite-dimensional optimization is a large, sparse linear program and was constructed using the open-source MATLAB-based software DTQP [48]. Then, MATLAB’s `linprog` solver using the interior-point method was found to be quite effective at solving the resulting linear program [49].

The time mesh was selected to be at hourly intervals as it is a reasonable assumption for the frequency at which control decisions (e.g., power plant’s power level would be changed) are made during realistic operation. The control decisions over these hourly intervals were assumed to be constant. With constant controls and linear dynamics, the zero-order hold (ZOH) method was used to discretize the dynamic constraints since there would be no discretization error [45]; a basic composite Euler forward method was chosen for quadrature. The ZOH method is particularly efficient to implement if matrices are time invariant. However, There are several locations in the formulation where time (really temperature) dependence would be useful, such as Eqs. (2.8) and (2.13).

This was particularly true for the state equations governing the flow of energy to and from the TES units described in Eq. (2.8) since it is desirable to allow the control variables ($p_{HS,in}$, $p_{CS,in}$, $p_{HS,out}$, $p_{CS,out}$) to be temperature-dependent to limit the amount of power flowing in or out of the TES units at certain temperatures – see Sec. 3.3 for more details. While an intuitive way is

directly expressing these values as time-varying, this would result in a time-varying linear (LTV) system, slowing down the problem construction step. An alternative but equivalent formulation was utilized by instead imposing time-dependent upper bounds on the relevant controls. This is demonstrated in the following notional example:

$$\dot{\xi} = a(t) \cdot u(t) \text{ and } 0 \leq u(t) \leq 1 \quad (\text{LTV case}) \quad (2.44a)$$

$$\dot{\xi} = \bar{u}(t) \text{ and } 0 \leq \bar{u}(t) \leq a(t) \quad (\text{LTI case}) \quad (2.44b)$$

In this formulation, Eqs. (2.6) and (2.7) are the relevant control constraints while Eq. (2.8) are expressed without any direct dependence on T_0 . When the upper bounds in Eqs. (2.6) and (2.7) are active, it can easily be shown that Eq. (2.8) assume the desired temperature-dependence.

2.2.3 Moving Prediction Horizons

As currently posed, the open-loop optimal control problem can be solved for any desired time horizon. As discussed in Sec. 2.1.5, the goal is to obtain results for one year of operation for use in the NPV calculations. This can be accomplished with a single optimization problem using an entire year’s worth of data.

However, despite this capability, solving a single horizon problem is not a realistic scenario as key environmental signals are not known with certainty so far into the future. In the real markets, signals such as electricity and fuel prices and ambient temperature are known to utility operators with reasonable accuracy only with limited foresight (e.g., 24 hours of future information [50]). To reflect this imperfect knowledge, which is crucial when determining the most profitable control strategy, the problem is also posed in as a sequence of shorter moving “prediction horizons” where information is known. Based on notions of model predictive control (MPC), this approach entails leveraging the knowledge of the future signals, despite being limited, to construct a tentative control strategy that is then updated when new information about the signals is available [51]. There are examples in the literature where similar control strategies based on limited future knowledge are applied to residential heating and cooling systems coupled with storage [52, 53].

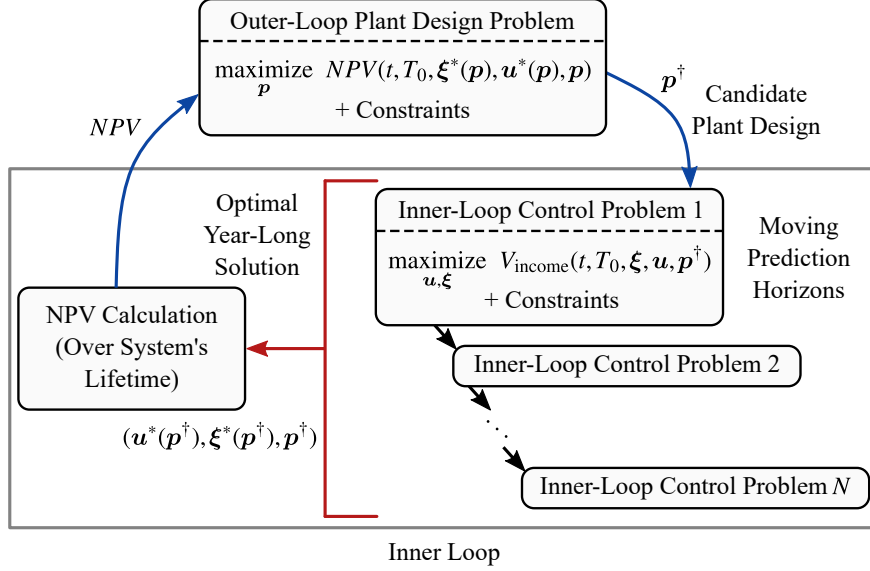


Figure 2.2: Overview of the nested control co-design optimization architecture for the moving prediction horizons approach.

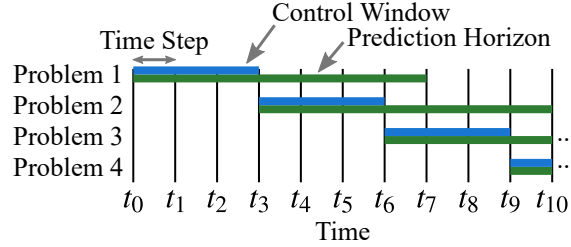


Figure 2.3: Moving prediction horizons and control window illustration.

When the moving horizons approach is taken, a nested CCD strategy formulation is used because separation is needed between the plant and control decisions [8,40,54]. As shown in Fig. 2.2, the inner loop is formulated as a sequence of control subproblems whose objective is to maximize the income generated by the system in Eq. (2.35) with respect to the states and controls (ξ, u) for fixed plant variables (p^\dagger) . The inner-loop solutions are then used in the objective function of the outer loop, which attempts to maximize NPV in Eq. (2.39).

Trade-offs in both control window and prediction horizon lengths (see Fig. 2.3) are explored in Sec. 3.4. The prediction horizon is the amount of time in the future information is known and includes many operational decisions to be made (e.g., from points t_0 to t_7 in the figure). The control window is the initial part of the prediction horizon that is implemented. After solution in the control window is implemented, the next optimization problem is solved starting where the previous con-

trol window ended. Understanding these trade-offs will help lead to implementable CCD-informed control solutions [55].

Chapter 3

Results and Discussion

This chapter presents several sets of results generated using the optimization model introduced in the previous sections with the purpose of validating its implementation and demonstrating some of its capabilities. Several TES technology configurations operating in different market scenarios and geographical locations will be examined. A detailed thermodynamic analysis has been conducted to generate the technical parameters identifying each of the TES configurations listed in App. A.2, which have then been modeled as integrated with the NGCC plant coupled with a Cansolv CC system [30] presented in the 2019 report by the National Energy Technology Laboratory (NETL), denoted case B31B [1]. Further details into the derivations of these parameters are in other publications [5,6].

The electricity and fuel prices and corresponding CO₂ tax used for this work represent future grid scenarios and have been generated by capacity expansion models built by Princeton University and the National Renewable Energy Laboratory (NREL) [19,56]. Temperature data from six of the more representative cities in the US was pulled from NREL's National Solar Radiation Database from 2018 [57]. Finally, the economic and financial values assumed for the calculation of NPV in these studies are reported in App. A.1.

When solving the optimization problem using the simultaneous strategy for an entire year, the setup and iterations of the required linear program takes between 20 and 50 s¹. Using the moving prediction horizons approach for a fixed plant, prediction horizon of 24 hours, and a control window of 12 hours, the computational cost is around 13 s and varies slightly depending on the moving horizon parameters. These computational times are reasonable for online implementation at the time scales considered.

¹The computer architecture was a workstation with an AMD 3970X CPU at 3.7 GHz and 128 GB 3200 MHz RAM.

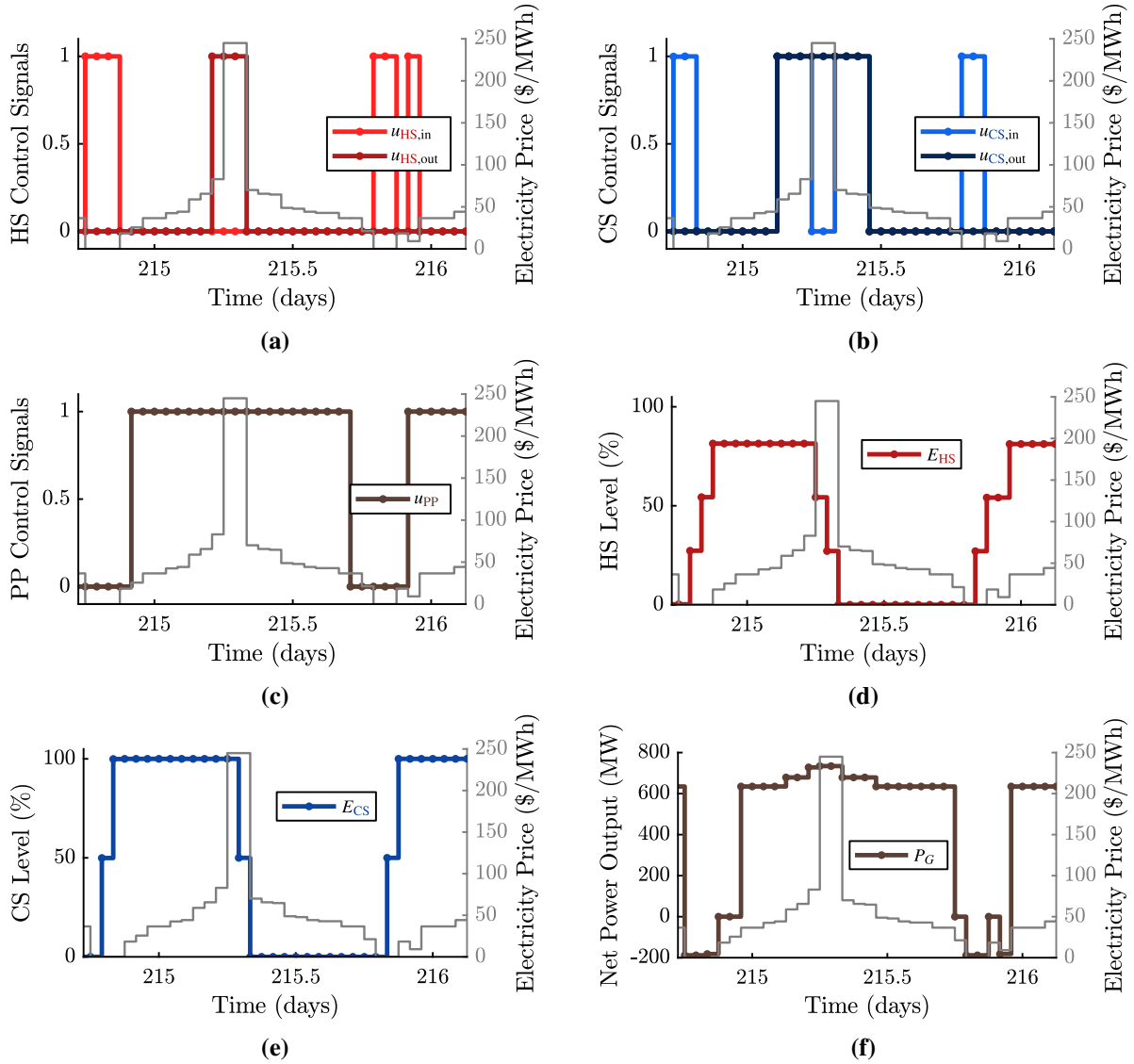


Figure 3.1: Snippet of an entire year’s solution illustrating the control, states, and net power output.

3.1 Control Strategy Results

The results presented in this section describe the workings of the control optimization to maximize NPV. In Fig. 3.1, a snippet of 33.5 hours of operation is shown from a year-long solution (i.e., prices and other signals are known and the controls must be determined simultaneously for an entire year) with hourly time resolution. Figures 3.1a–3.1c show all 5 of the control variables (u from Eq. (2.41)) governing the system, normalized with respect to their upper bounds (e.g., $u_{HS,in} = p_{HS,in}/(\mu_{HS,in} \cdot P_{HS,in})$). Figures 3.1d–3.1e respectively show the HS and CS level, two state

variables in the model (see Eq. (2.42)). Finally, Fig. 3.1f shows the net power output to the grid, in which we can recognize several discrete and typical operation modes.

In the first few hours, while the electricity prices are lowest, both the HS and CS units are being charged as the normalized control variables ($u_{HS,in}, u_{CS,in}$) are equal to unity in Figs. 3.1a–3.1b, and the TES units levels (E_{HS}, E_{CS}) in Fig. 3.1d–3.1e increase. The TES technology configuration chosen allows for charging while the PP is offline, and that is why in this mode, the control variable to the PP (u_{PP}) is equal to zero in Fig. 3.1c and the net power output in Fig. 3.1e is negative, meaning that electricity is consumed from the grid rather than delivered. Successively, after one time-interval in which the entire system is offline, the PP goes online in neutral mode for a few time-steps, which is represented by $u_{PP} = 1$ and all other control variables equal to zero. Then, when electricity prices are higher, it becomes profitable to access the system’s boosting mode, which consists in charging and discharging the CS at the same time (i.e., $u_{CS,in} = u_{CS,out} = 1$ in Fig. 3.1b). Because the power increase from discharging the CS is larger than the penalty for charging it, the boosting mode results in a slight increase in the system’s net power output as compared with the PP neutral mode. In principle, the model does not prevent the HS from also operating in boosting mode, but because the HS generally requires more power to charge than it can generate, the boosting mode is only effective with the CS.

In the region of the plots where the electricity prices are highest, both TES units are depleted to output the maximum amount of power to the grid. This is shown by the larger power output in Fig. 3.1e, by the control variables ($u_{HS,out}, u_{CS,out}$) being equal to unity in Figs. 3.1a–3.1b, and by the TES levels decreasing in Figs. 3.1d–3.1e. Successively, as the electricity prices are still high but the TES units are depleted, the system is again operated in boosted mode before descending back to neutral and finally beginning another charging cycle with the PP off. For similar figures showing a more extended control solution in time, see App. B.

It appears that the optimal control solution returned from the model reflects the behavior expected from each of the system’s submodules in order to maximize the revenue generated. As additional evidence, Fig. 3.2 shows the correlation between the electricity prices and each of the

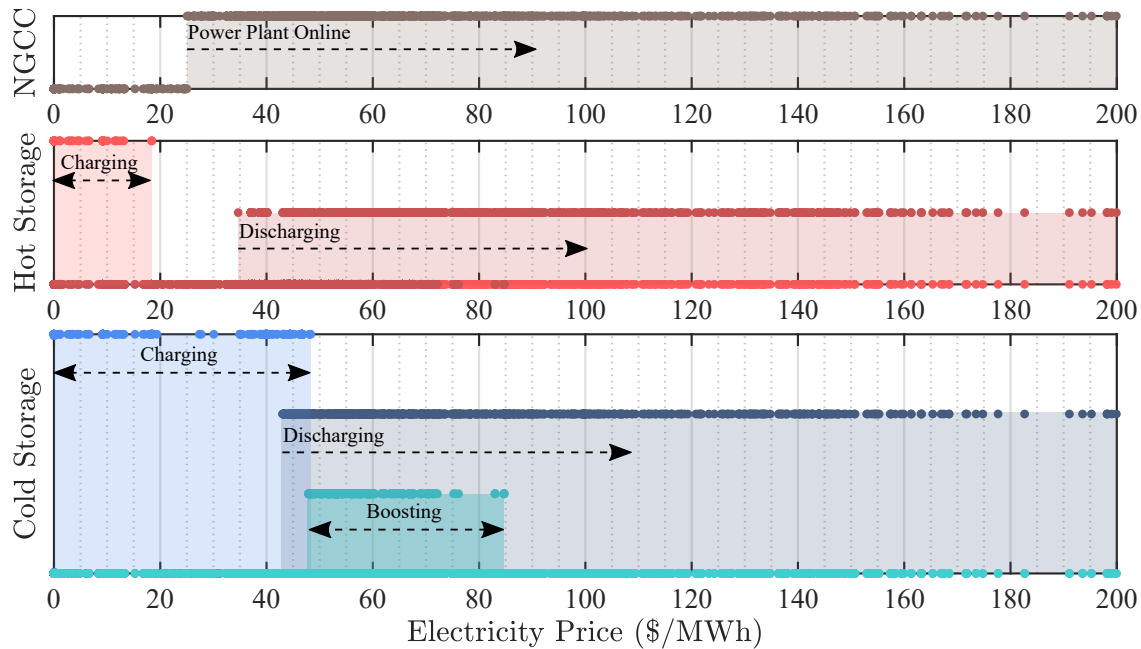


Figure 3.2: The optimization results show certain correlation between typical operational modes of the system and the electricity prices.

operating modes of the system for an entire year of operation, using a TES configuration that can charge with the PP offline, a fixed design including 4 hours of TES, nominal energy transfer rates for HS and CS, respectively, and market conditions specified by the “HighWindTax” market scenario provided by the GenX capacity expansion model [19].

As discussed, there is a distinct electricity price value – the break-even point – above which operating the PP becomes profitable, and in this scenario, this is around 25 \$/MWh. The control decisions concerning operating the HS are also fairly intuitive: charging occurs at prices between 0 \$/MWh and 18 \$/MWh while discharging becomes advantageous at prices above 34.5 \$/MWh. While the correlation between the operation modes is relatively intuitive for the PP and the HS, the optimal control decisions for the CS are slightly more complex, in part due to the additional degree of freedom represented by the boosting mode previously described in Sec. 1.4, but also because contrary to the HS, discharging the CS results in additional fuel consumption and a decreased CC rate – as explained in Sec. 1.4. These two factors make an intuitive correlation between the operation modes of the CS and the electricity prices difficult to draw, and significant overlap between the price regions is observed. In addition to electricity prices at any given time, the optimal operation

mode for the CS is likely more affected by considerations related to current storage availability, future pricing signals, and additional costs associated with consuming more fuel and emitting more CO₂ for discharging the CS.

3.2 Justifications for Open-loop Control Co-design

Results of the previous section present insights on the optimal control solution for an NGCC power plant equipped with CC and TES in response to typical market signals (mainly electricity prices). While a specific correlation between the electricity pricing signals and the optimal operation modes of the system can be generally drawn (potentially leading to a heuristics-based control strategy), here, the case is made that the CCD approach taken in this work is appropriate to achieve the system's best economic performance and therefore most fair evaluation.

To make this case, intuition-based control heuristics for the system are compared with the model's CCD optimal solution. A fundamental assumption underlying these heuristics is that electricity prices generally show daily periodicity so that each day can be solved as an independent problem. Then, a simple strategy can be designed as follows, assuming a fixed plant design and hourly control decisions:

1. The daily time-intervals are sorted based on the value taken by the electricity prices: depending on the selected TES capacity, the lowest intervals are assigned to charging, and the highest to discharging the TES units
2. The remaining time intervals are assigned to neutral mode if they are above the break-even line or to boosting if more profitable
3. At the time periods in which the electricity prices are below the break-even point, the PP is shut off

While relatively simple and surely expandable to account for more nuanced situations, the heuristics presented can be a somewhat effective starting point for making operation decisions about the TES system. However, there are some critical flaws that are difficult to address and which

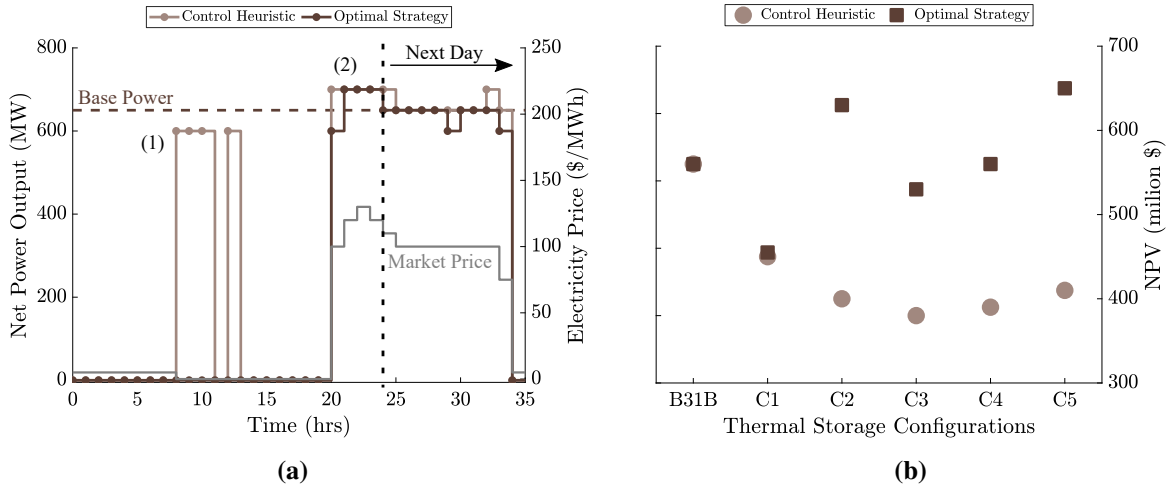


Figure 3.3: A comparison with an heuristic-based control strategy shows the benefits of the optimization-based approach in handling specific situations (a), and returning more accurate results (b).

can make this approach ineffective and inaccurate. First, these heuristics consider the **HS** and **CS** as a single unit. This implies that they always operate in the same modes and that their storage capacities are identical. While generally similar factors influence the decisions to operate the TES units – see Sec. 1.4 – this needs not always be the case, and more importantly, as discussed in more detail in Sec. 3.5, it turns out the optimal storage capacities for **HS** and **CS** are usually substantially different. Figure 3.3a shows a snippet of 36 hours of operation comparing the solutions returned by the heuristics-based approach and the optimization model: assuming the TES capacity for **HS** and **CS** are both 4 hours, two additional fundamental flaws in the heuristics become clear: this strategy can often be ineffective, choosing to charge the storage units, and in this case turning on the **NGCC** plant, when the prices are extremely low, incurring in enormous operation costs (indicated as ‘1’ in Fig. 3.3a); it also lacks in accuracy, discharging more thermal energy that is allowed by the storage capacity – indicated as ‘2’ in the image – because successive days are considered as independent problems.

These are some of the reasons justifying an optimization-based approach to the dynamic control of the TES technology in favor of a heuristics-based approach. Figure 3.3b shows a comparison between 5 TES configurations and an **NGCC** power plant with **CC** but not TES (i.e., B31B): not only using the optimization model results in a general positive difference between the TES

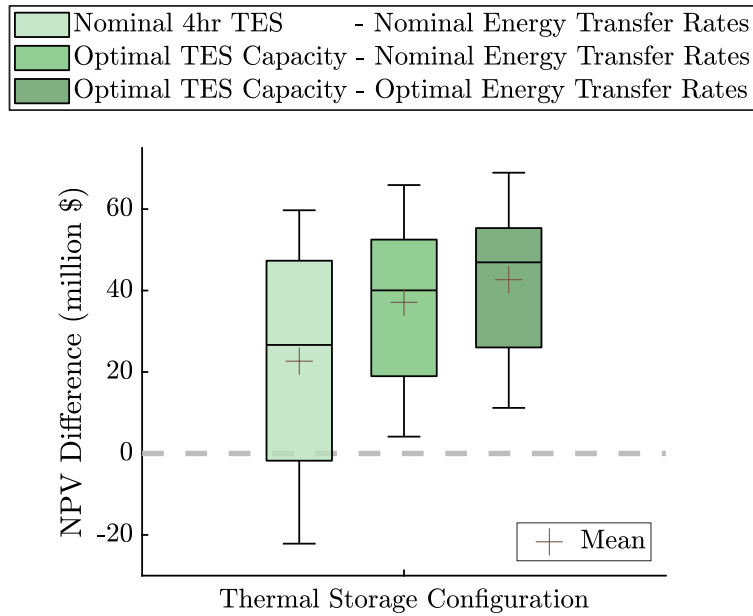


Figure 3.4: Motivation for open-loop control co-design optimization.

technologies and B31B, but the relationships among the technologies themselves are also radically different.

In addition to realizing the optimal control of the TES technology, appropriate design decisions such as storage capacity and energy transfer rates for the HS and CS are crucial when assessing this technology. This is due to a delicate balance between performance and capital investment, which is also technology and scenario dependent. Figure 3.4 shows the difference in economic performance between a TES technology and B31B in various market scenarios under three different design conditions: 1) the TES capacity is set for 4 hours for both units, based on the observation that often the electricity prices show daily peaks of that duration, and the energy transfer rates are the nominal values. 2) the TES capacities are included as optimization variables, but the energy transfer rates are still fixed, resulting in an increase in average value by 14 million \$. 3) both capacity and energy transfer rates are considered in the full CCD problem, which on average increases the NPV by 20 million \$. Similar differences are generally encountered while examining other configurations and motivate the presented CCD approach to evaluate the TES technology accurately.

3.3 Temperature-dependence Results

We now look at validating temperature dependence within the model and show the impact of location characteristics on the examined system. Temperature dependence was included in the model to represent the systems more accurately in real-world scenarios: it is known that power generation systems like NGCC power plants are susceptible to ambient conditions [58]. In addition, the operation of the TES units is also impacted by temperature. In particular, concerns regarding the effectiveness of CS operating at temperatures below a certain design point can be investigated using this model.

Cold Storage Operation Validation

A concern regarding the CS operation at temperatures below its design point is in the potential for ice formation in the ducting and physical damage to the unit. As a safe assumption to avoid these issues (and as a more accurate assessment of the technology in colder climates), CS utilization is limited to temperatures above 0°C, with partial restrictions from 0°C to the system's design point (15°C). Figure 3.5 validates the implementation of this assumption in the model; it shows the signal to use the CS boosting mode in two very different US geographical locations (Fargo and San Diego), during a year-long operation period. The market signals provided to generate these sets of results are identical, as well as the plant design; only the temperature signals identifying each of the US locations are different. With these assumptions, it is shown that a system deployed in Fargo, which is described by large seasonal temperature fluctuations and remarkably cold winters, will only be able to access the CS full capabilities during the warmer summer months. On the other hand, in a location like San Diego, the CS can be virtually used all year round because of its milder climate and higher temperatures.

System Performance Validation

The entire system is expected to be affected by ambient temperature, not just the CS. In particular, the efficiency of the PP and the HS are expected to significantly decrease as temperature increases, and this characteristic has been integrated within the model. Figure 3.6 shows the im-

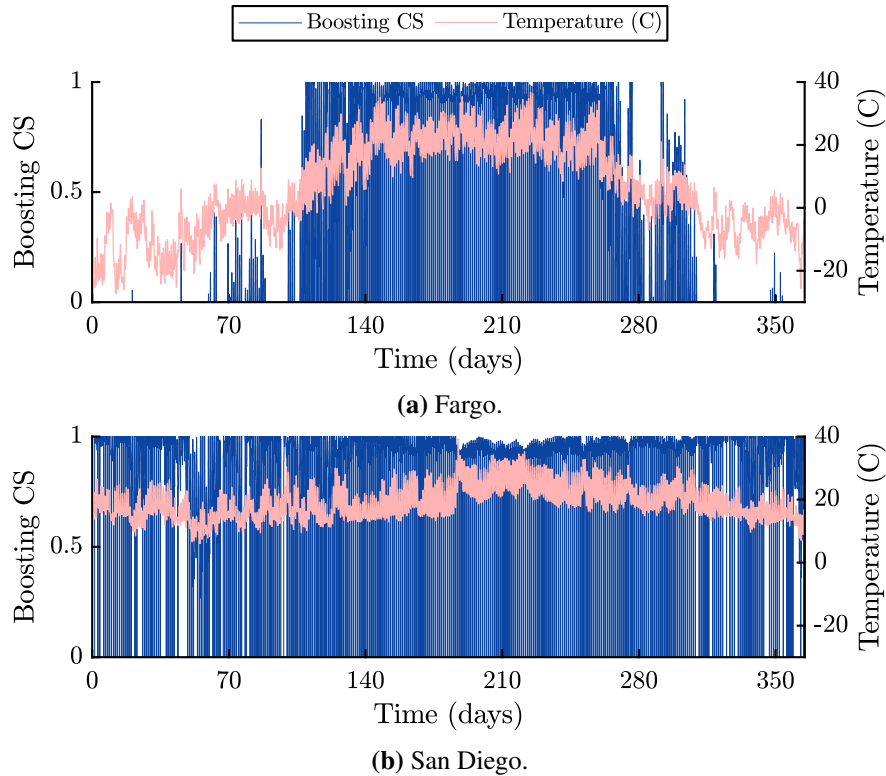


Figure 3.5: CS boosting operation for two different locations demonstrating temperature-dependent optimal operation.

impact of temperature on the NPV of both a PP with CC and TES, as well as a base plant which is equipped with CC but no TES (denoted B31B). For this study, the techno-economic input signals are kept the same, while recorded time-varying temperature signals are selected to represent the US cities shown.

For these results, CCD optimization was conducted to make a fair assessment of these systems' optimal design decisions and performance depending on their location. As shown in Fig. 3.6, while NPV's for both B31B and the TES configuration noticeably decrease in warmer climates, the difference between the PP equipped with TES and the base plant tends to increase with average temperature. This trend is generally observed in Fig. 3.6, although since the model evaluates the effects of temperature at each time step, it is the entire temperature distribution affecting the performance of the system rather than just the mean value. For example, the system might perform better in Fargo than in Salt Lake City, despite the higher average annual temperature in the latter location.

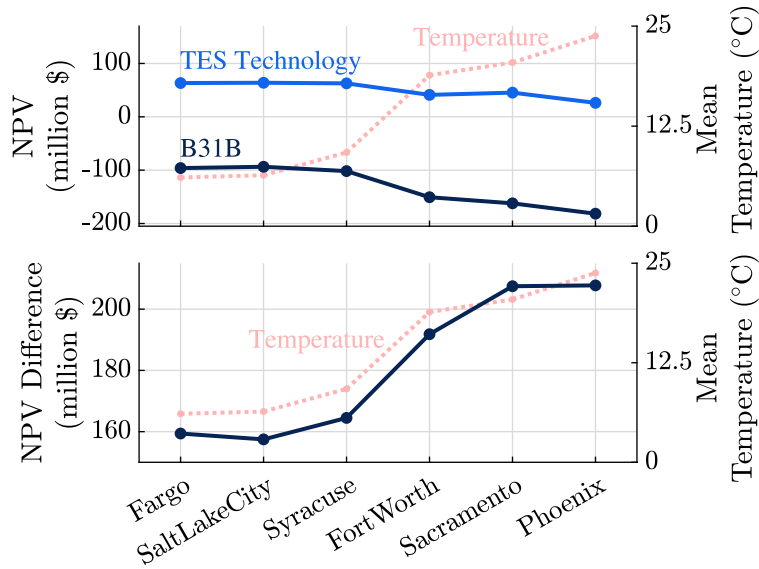


Figure 3.6: Comparing optimal net present value results for several locations and correlating them with their mean temperatures.

3.4 Moving Prediction Horizons Strategy Results

Introduced in Sec. 2.2.3, a moving prediction horizons (MPH) is a pragmatic approach to the control of the system discussed in this thesis involving limited future foresight of the techno-economic signals upon which the optimal control strategy depends. Nonetheless, it will be shown that under realistic circumstances, the MPH approach ensures an economic performance extremely close to the results with perfect foresight and could be a suitable candidate for online control operation of an NGCC plant with CC and TES.

First, to better illustrate an MPH solution, Fig. 3.7 shows the net power output of the system for a few time intervals. The top row shows four successive intervals, each with its own control trajectory. The optimal strategy is computed for a total of 6 hours in advance (prediction horizon) but is updated every 3 hours (control window) because it is assumed that new information about the market is provided. On the bottom, the four intervals plotted above are shown as they compose the complete control strategy.

In Fig. 3.8, we can conclude that for certain values of the prediction horizon and control window, an MPH is an effective strategy for this system. Several different control window lengths were examined, and we observe NPV convergence towards the best possible value (simultaneous

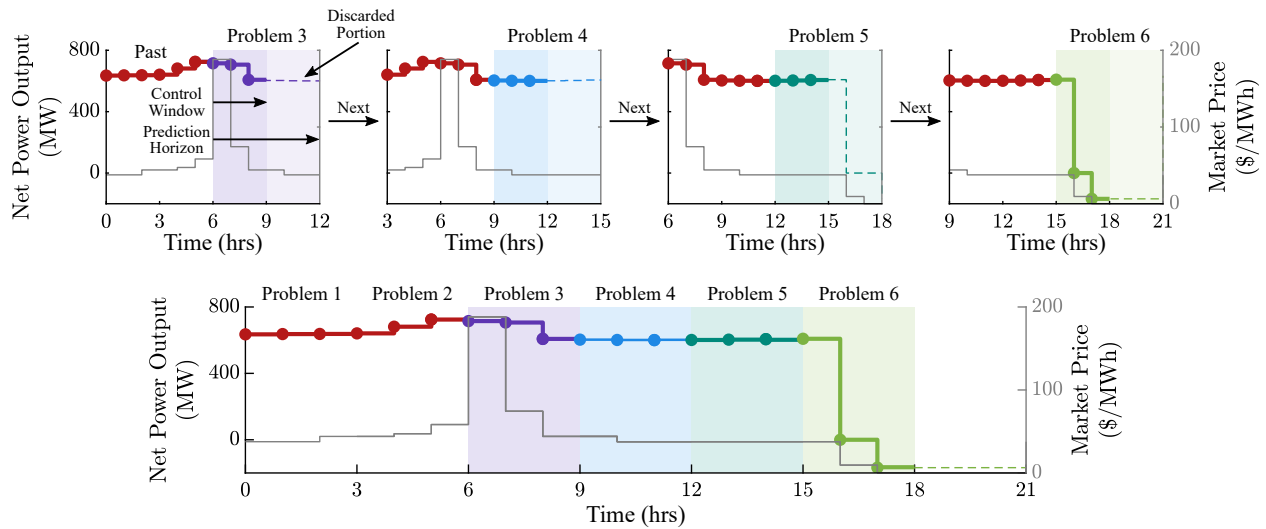


Figure 3.7: Illustration of the moving prediction horizon approach with a prediction window of 6 hours and control window of 3 hours.

optimization of the entire year, i.e., prediction horizon is 8760 hours) in all cases. Marked with ‘1’ in the figure, assuming accurate estimates of the electricity prices are available 24 hours in advance (which is usually true in most markets), we can observe solutions with control windows between 1–12 hours are close to the maximum NPV line. Even if signals are available only half a day in advance (i.e., 12-hr prediction horizon, marked with ‘2’ in the figure), any strategy with a smaller control window still performs well. The success of the MPH approach can at least partially be explained by the general daily periodic nature of electricity prices, as well as by the TES capacities usually encountered by these systems being rarely above 12 hours. Due to these two factors, not much prior knowledge of future signals is required to operate this system effectively.

3.5 TES Technology Comparison Results

One of the more valuable features of the optimization model described in this thesis is its versatility assessing a wide range of different PP, CC, HS, and CS technologies without much additional work. Here, we demonstrate this versatility with the assessment of two TES technology configurations compared with NETL’s NGCC plant with CC (B31B). These configurations are examined using four future market scenarios provided by the Princeton capacity expansion model [19].

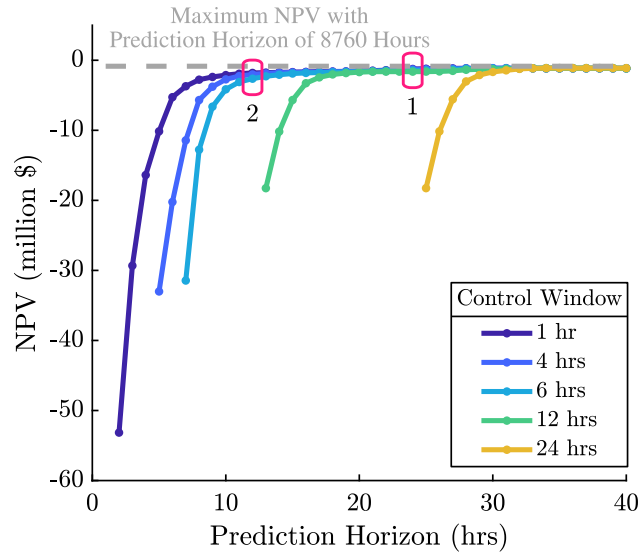


Figure 3.8: Net present value results for various prediction horizon and control window lengths in the moving prediction horizon approach compared to the maximum NPV for this scenario.

The TES configurations examined are based on different thermodynamic principles, which result in some different operational constraints. The ‘IPTE’ configuration is constructed by integrating B31B with an HS unit which is charged by directly pulling steam from the PP. This configuration requires the PP to be online to operate in this mode. Conversely, the ‘ER’ configuration uses resistive heating and electricity either from the grid or subtracted from the NGCC gross output to charge its HS. For this reason, while the ER HS unit inflicts a more significant power penalty for charging (89% more than IPTE), it has the advantage of being able to charge while the PP is offline and to be significantly cheaper in terms of HS medium cost (by 78%). Conversely, the CS is similar for both TES configurations: it is based on an ammonia vapor compression cycle powered through electricity, and it can therefore also be charged independently of the PP. These extra operational degrees of freedom are implemented in the model by removing the inequality constraints in Eq. (2.16a). Again, see App. A.2 for the parameters defining each configuration. For additional details on the specific technologies and their modeling, see Refs. [5, 6].

Figure 3.9a compares the optimal NPV of the technologies across the market scenarios. Although we notice a relatively wide range of results, ER appears to be consistently the most profitable configuration analyzed, which can be explained by both its relatively low capital investment

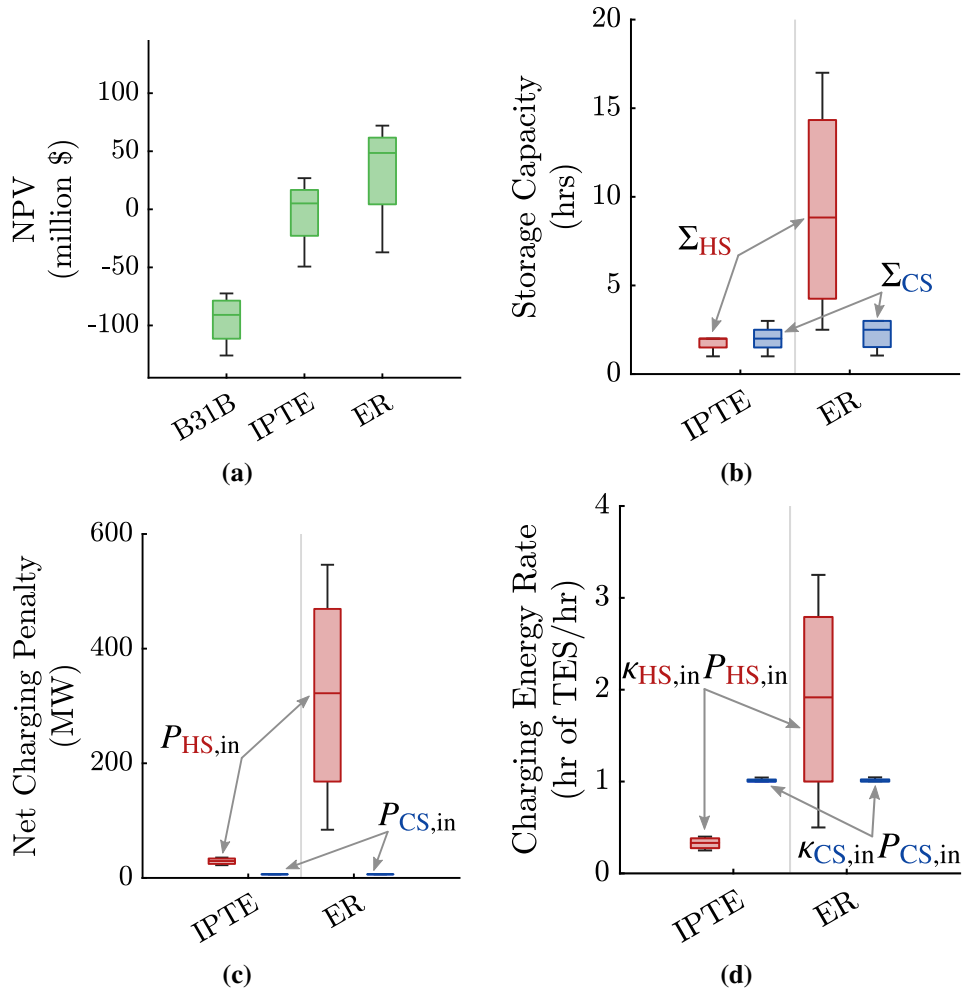


Figure 3.9: Comparing three different system configurations under several market scenarios including (a) net present value; (b) optimal storage capacities Σ_{HS} and Σ_{CS} ; (c) optimal TES charging power penalties $P_{HS,in}$ and $P_{CS,in}$; and (d) equivalent optimal thermal energy transfer to the TES units.

and the optimal plant sizing decisions shown in Figs. 3.9b and 3.9c. The storage capacity values in Fig. 3.9b are represented in units of time, after being normalized with respect to the power required to run the HS and CS.

We first notice how the HS design decisions are significantly different between the IPTE and ER configurations and generally point towards a much larger optimal storage capacity and net charging power penalty for the HS ($P_{HS,in}$) for the latter. This observation can be explained by: 1) the lower cost for the ER's HS medium, and 2) its ability to charge independently of the plant coupled with the nature of future electricity prices. The latter reason is particularly insightful in the context of future electricity markets with high renewable penetration: the higher penalty

associated with charging the ER becomes irrelevant when the electricity prices are close to zero due to renewable's overgeneration [6]. Under these conditions, the overgenerated electricity can be stored directly from the grid within a large HS and at a high rate (demonstrated by large optimal HS normalized charging energy rate in Fig. 3.9d) to then take advantage of when the renewables are offline, and the prices are peaking. For the CS, the results for the two different configurations do not vary much as the CS unit is similar in both. A set of plant optimization variables is not shown in Fig. 3.9, namely the maximum energy transfer rates out of the TES units $P_{HS,out}$ and $P_{CS,out}$: under the current assumptions, their optimal values were always the maximum allowed.

Many other configurations and market scenarios were explored using this CCD optimization model in Refs. [5,6].

Chapter 4

Conclusion

4.1 Summary

In this thesis, an optimization model was constructed to help address important design and operation questions for a novel system combining natural gas NGCC power plants with carbon capture CC and thermal energy storage TES.

The motivation behind the conceptualization of this system is the expected evolution of the electricity markets towards a carbon-neutral electricity grid heavily penetrated by renewable energy sources, resulting in highly variable electricity prices and demand. In this context, there will be an opportunity for clean, flexible, and cheap fossil fuel-based generators, such as NGCC plants with CC, to complement renewable generation. However, while recent work has demonstrated that high CO₂ rates are achievable, challenges due to high capital costs, flexibility limitations, and the parasitic load imposed by CC systems onto NGCC power plants have so far prevented its commercialization. Coupling TES units with CC and NGCC would allow storing thermal energy into the TES units when the electricity prices are low, either by subtracting it from the NGCC or by extracting it from the grid and to discharge thermal power at peak prices, from the TES to offset the parasitic load of the CC system, and from the TES for chilling the inlet of the NGCC combustion turbine, increasing the output of the cycle beyond nominal value.

The need for integrated design, control co-design in particular, is demonstrated for the considered system. The thermal energy storage elements and power plant require a dynamics-focused approach and how they are exercised is a critical decision that affects profitability and overall technology assessment. The proposed open-loop optimal control problem for this system is efficiently solved as a large-sparse linear program for an entire year at once or utilizes a more realistic, information-limited moving prediction horizons approach to investigate implementable operation. Optimal system control is generally not enough to realize its full economic potential due to several

critical plant decisions, including storage capacities and maximum energy transfer rates. Often driven by trade-offs in their capital cost versus the additional profit attained, the optimal plant sizing decisions change depending on the configuration and environmental signals such as (both current and future) electricity prices and location temperature.

After detailed analysis, the technology shows remarkable promise in that it outperforms NGCC power plants with state-of-the-art CC systems in many of the scenarios evaluated. The best overall TES technology solution relies on cheap excess grid electricity from renewable sources to charge the TES units – the HS via resistive heating and the CS through an ammonia-based vapor compression cycle.

4.2 Future Work

In addition to the current capabilities of the optimization model, which have been described in this thesis, future work could attempt to implement several updates to improve the model in several aspects. Following is a short list of some of the envisioned improvements:

Market Uncertainty Considerations

One of the most appealing features of the model in this thesis is the more realistic representation of limited information signals provided by the moving horizons approach described in Secs. 2.2.3 and 3.4. Although this solution constitutes a more realistic approach than assuming perfect foresight of future signals, in reality even the limited future information available to utilities might come with a particular uncertainty (i.e., what is given is not exactly what happens). Future work will attempt to integrate this uncertainty into the model, understand its impacts on economic performance and optimal solutions, and account for it robustly to guarantee effective system performance under uncertainty. Additionally, data generated from these studies will be analyzed to better understand optimal operation, potentially leading to feedback control solutions [55].

Carbon Capture System Dynamics

As explained in the optimization problem formulation in Sec. 2.1.3, the CC system currently is implemented in the model as always operating when the PP is operating. While for the work presented in this thesis this is likely a reasonable approximation, in general, it is expected for CC systems to be described by different dynamics from NGCC plants. A solution is then to modify the current model to include the CC's capture rate as an additional state variable in the model similar to Eq. (2.42). This addition would give the opportunity to associate the CC system with its own dynamic equation but also explore new operation modes, including shutting off the CC, bypassing it and venting the CO₂ if profitable, and looking into pre-warming the CC by using steam generated from the HS while the NGCC is offline to effectively reduce its start-up time.

Other Improvements to the Optimization Model

In Sec. 2.1.5, the economic model for calculating NPV was presented. While this model was sufficiently accurate to evaluate the economic performance of the integrated system with different environmental as well as technology assumptions, the calculation of NPV can be made more nuanced to reflect more accurately the capital investments necessary to finance a system like that described in this work. For instance, rather than assuming all capital investments are made at once before the operation of the system begins, a construction period, annual loan installments with appropriate interests, and tax payments can be implemented in a more complete discounted cash-flow analysis which would ultimate results in more accurate estimates of NPV.

Continuing, in Sec. 2.1.5 it was presented how the computational expenses of representing the system's operation over its entire lifetime (here assumed to be 30 years) at hourly resolution were decreased by computing the optimization over one year and then assuming an identical control strategy in the following years. This approach would be completely effective if the external signals remained identical throughout the system's lifetime. However, since in Eq. (2.36) we enforced a rate at which some of the signals (electricity and fuel prices) are expected to change annually, it cannot be guaranteed the optimal control strategy would remain identical to that including the original signals. Although some testing has shown that in most cases, the assumption made in

Eq. (2.36) is reasonable, yielding conservative results, future work should consider and characterize its implications in more detail towards a more accurate financial assessment of the technology.

Finally, while not explicitly covered in the context of this thesis, another current assumption in the model is that changes to fuel prices (natural gas in this study) occur relatively infrequently and are not a major factor dictating the operation of the system. However, in real-world energy markets, fluctuations in the price of fuels such as natural gas can significantly impact utility operators. Considerations regarding the impact of such variability in natural gas prices would make the model more accurate and potentially open up additional arbitrage opportunities.

Solution Efficiency Improvements to the Optimization Model

As discussed in Sec. 2.2.3, when the moving predictions horizon is the chosen approach for the control strategy of the system, the CCD problem is formulated as a nested optimization problem. Despite the inner loop analysis being comprised of series of linear subproblems which can be efficiently solved, the function wrapping these subproblems cannot be regarded as linear itself but rather as a black-box, input-output type of function. Therefore, an appropriate strategy must be selected to solve the outer-loop optimization problem so that the calls to the (expensive) inner loop are limited. Both gradient-free and surrogate-based optimization methods have been considered as potential solutions, as well as a hybrid approach combining the two.

Bibliography

- [1] R. E. James III, D. Kearins, M. Turner, M. Woods, N. Kuehn, and A. Zoelle, “Cost and performance baseline for fossil energy plants volume 1: bituminous coal and natural gas to electricity,” National Energy Technology Laboratory, Tech. Rep. NETL-PUB-22638, Sep. 2019, doi: [10.2172/1569246](https://doi.org/10.2172/1569246)
- [2] J. D. Jenkins, Z. Zhou, R. Ponciroli, R. B. Vilim, F. Ganda, F. de Sisternes, and A. Botterud, “The benefits of nuclear flexibility in power system operations with renewable energy,” *Applied Energy*, vol. 222, pp. 872–884, Jul. 2018, doi: [10.1016/j.apenergy.2018.03.002](https://doi.org/10.1016/j.apenergy.2018.03.002)
- [3] M. A. Gonzalez-Salazar, T. Kirsten, and L. Prchlik, “Review of the operational flexibility and emissions of gas- and coal-fired power plants in a future with growing renewables,” *Renewable and Sustainable Energy Reviews*, vol. 82, no. 1, pp. 1497–1513, Feb. 2018, doi: [10.1016/j.rser.2017.05.278](https://doi.org/10.1016/j.rser.2017.05.278)
- [4] U.S. Energy Information Administration, “Levelized costs of new generation resources in the annual energy outlook 2022,” 2022. [Online]. Available: https://www.eia.gov/outlooks/aeo/pdf/electricity_generation.pdf
- [5] B. J. Limb, E. Markey, R. Vercellino, S. Garland, M. Pisciotta, P. Psarras, D. R. Herber, T. Bandhauer, and J. C. Quinn, “Economic viability of thermal energy storage on natural gas power plants with carbon capture,” (*submitted to*) *Journal of Energy Storage*, 2022.
- [6] E. Markey, “Economic impact of resistively heated hot thermal storage and vapor compression cold thermal storage on natural gas power with carbon capture in future electricity markets,” M.S. Thesis, Colorado State University, Fort Collins, CO, USA, 2022.
- [7] J. Wilcox, *Carbon Capture*. Springer, 2012, doi: [10.1007/978-1-4614-2215-0](https://doi.org/10.1007/978-1-4614-2215-0)

- [8] A. K. Sundarrajan and D. R. Herber, “Towards a fair comparison between the nested and simultaneous control co-design methods using an active suspension case study,” in *American Control Conference*, May 2021, doi: [10.23919/ACC50511.2021.9482687](https://doi.org/10.23919/ACC50511.2021.9482687)
- [9] H. Shaftel, S. Callery, R. Jackson, and D. Bailey, “Climate change: How do we know?” 2022. [Online]. Available: <https://climate.nasa.gov/evidence/>
- [10] IPCC, “Climate change 2022: mitigation of climate change,” Cambridge University Press, Contribution of Working Group III to the Sixth Assessment Report of the Intergovernmental Panel on Climate Change, 2022, doi: [10.1017/9781009157926](https://doi.org/10.1017/9781009157926)
- [11] “Paris agreement,” United Nations, Paris, France, Tech. Rep., 2016. [Online]. Available: <https://unfccc.int/documents/184656>
- [12] International Energy Agency, “Net zero by 2050,” IEA, Paris, France, Tech. Rep., 2021. [Online]. Available: <https://www.iea.org/reports/net-zero-by-2050>
- [13] “The long term strategy of the United States: Pathways to net-zero greenhouse gas emissions by 2050,” United States Department of State and the United States Executive Office of the President, Washington DC, USA, Tech. Rep., Nov. 2021. [Online]. Available: <https://unfccc.int/documents/308100>
- [14] “Annual energy outlook 2021,” U.S. Energy Information Administration, Washington, DC, USA, Tech. Rep., Feb. 2021. [Online]. Available: <https://www.eia.gov/outlooks/archive/aeo21/>
- [15] U.S. Energy Information Administration, “Coal will account for 85% of U.S. electric generating capacity retirements in 2022,” Jan. 2022. [Online]. Available: <https://www.eia.gov/todayinenergy/detail.php?id=50838>
- [16] —, “Solar power will account for nearly half of new U.S. electric generating capacity in 2022,” Jan. 2022. [Online]. Available: <https://www.eia.gov/todayinenergy/detail.php?id=50818>

- [17] C. Stark, J. Pless, J. Logan, E. Zhou, and D. J. Arent, “Renewable electricity: insights for the coming decade,” Joint Institute for Strategic Energy Analysis, Golden, CO, USA, Tech. Rep. NREL/TP-6A50-63604, Feb. 2015, doi: [10.2172/1176740](https://doi.org/10.2172/1176740)
- [18] T. Rintamäki, A. S. Siddiqui, and A. Salo, “Does renewable energy generation decrease the volatility of electricity prices? An analysis of Denmark and Germany,” *Energy Economics*, vol. 62, pp. 270–282, Feb. 2017, doi: [10.1016/j.eneco.2016.12.019](https://doi.org/10.1016/j.eneco.2016.12.019)
- [19] J. D. Jenkins, S. Chakrabarti, F. Cheng, and N. Patankar, “Summary report of the GenX and PowerGenome runs for generating price series (for ARPA-E FLECCS project),” Dec. 2021, doi: [10.5281/zenodo.5765798](https://doi.org/10.5281/zenodo.5765798)
- [20] P. D. Lund, J. Lindgren, J. Mikkola, and J. Salpakari, “Review of energy system flexibility measures to enable high levels of variable renewable electricity,” *Renewable and Sustainable Energy Reviews*, vol. 45, pp. 785–807, May 2015, doi: [10.1016/j.rser.2015.01.057](https://doi.org/10.1016/j.rser.2015.01.057)
- [21] D. P. Hanak and V. Manovic, “Linking renewables and fossil fuels with carbon capture via energy storage for a sustainable energy future,” *Frontiers of Chemical Science and Engineering*, vol. 14, no. 3, pp. 453–459, 2020, doi: [10.1007/s11705-019-1892-2](https://doi.org/10.1007/s11705-019-1892-2)
- [22] U.S. Energy Information Administration, “Electricity data browser,” 2022. [Online]. Available: <https://www.eia.gov/electricity/data/browser/>
- [23] International Energy Agency, “World energy outlook 2021,” IEA, Paris, France, Tech. Rep., 2021. [Online]. Available: <https://www.iea.org/reports/world-energy-outlook-2021>
- [24] L. Branchini, *Waste-to-Energy and Gas Turbine: Hybrid Combined Cycle Concept*. Springer International Publishing, 2015, pp. 57–70, doi: [10.1007/978-3-319-13608-0_5](https://doi.org/10.1007/978-3-319-13608-0_5)
- [25] M. Boyce, “Combined cycle power plants,” in *Combined Cycle Systems for Near-Zero Emission Power Generation*, ser. Woodhead Publishing Series in Energy, A. D. Rao, Ed. Woodhead Publishing, 2012, pp. 1–43, doi: [10.1533/9780857096180.1](https://doi.org/10.1533/9780857096180.1)

- [26] S. Babaee and D. H. Loughlin, “Exploring the role of natural gas power plants with carbon capture and storage as a bridge to a low-carbon future,” *Clean Technologies and Environmental Policy*, vol. 20, pp. 379–391, 2018, doi: [10.1007/s10098-017-1479-x](https://doi.org/10.1007/s10098-017-1479-x)
- [27] P. Psarras, J. He, H. Pilorgé, N. McQueen, A. Jensen-Fellows, K. Kian, and J. Wilcox, “Cost analysis of carbon capture and sequestration from U.S. natural gas-fired power plants,” *Environmental Science & Technology*, vol. 54, no. 10, pp. 6272–6280, 2020, doi: [10.1021/acs.est.9b06147](https://doi.org/10.1021/acs.est.9b06147)
- [28] D. S. H. Wong and S. Jang, *Plantwide design and operation of CO₂ capture using chemical absorption*, ser. Process Systems and Materials for CO₂ Capture: Modelling, Design, Control and Integration. Wiley, 2017, ch. 16, pp. 427–445, doi: [10.1002/9781119106418.ch16](https://doi.org/10.1002/9781119106418.ch16)
- [29] K. Goto, K. Yogo, and T. Higashii, “A review of efficiency penalty in a coal-fired power plant with post-combustion CO₂ capture,” *Applied Energy*, vol. 111, pp. 710–720, Nov. 2013, doi: [10.1016/j.apenergy.2013.05.020](https://doi.org/10.1016/j.apenergy.2013.05.020)
- [30] A. Singh and K. Stéphenne, “Shell Cansolv CO₂ capture technology: achievement from first commercial plant,” *Energy Procedia*, vol. 63, pp. 1678–1685, 2014, doi: [10.1016/j.egypro.2014.11.177](https://doi.org/10.1016/j.egypro.2014.11.177)
- [31] Bui, M., et al., “Carbon capture and storage (CCS): the way forward,” *Energy & Environmental Science*, vol. 11, no. 5, pp. 1062–1176, 2018, doi: [10.1039/c7ee02342a](https://doi.org/10.1039/c7ee02342a)
- [32] A. M. Abdilahi, M. W. Mustafa, S. Y. Abujarad, and M. Mustapha, “Harnessing flexibility potential of flexible carbon capture power plants for future low carbon power systems: review,” *Renewable and Sustainable Energy Reviews*, vol. 81, no. 2, pp. 3101–3110, Jan. 2018, doi: [10.1016/j.rser.2017.08.085](https://doi.org/10.1016/j.rser.2017.08.085)
- [33] N. M. Dowell and N. Shah, *Multi-period design of carbon capture systems for flexible operation*, ser. Process Systems and Materials for CO₂ Capture: Modelling, Design, Control and Integration. Wiley, 2017, ch. 17, pp. 447–462, doi: [10.1002/9781119106418.ch17](https://doi.org/10.1002/9781119106418.ch17)

- [34] S. M. Cohen, G. T. Rochelle, and M. E. Webber, "Optimal operation of flexible post-combustion CO₂ capture in response to volatile electricity," *Energy Procedia*, vol. 4, pp. 2604–2611, 2011, doi: [10.1016/j.egypro.2011.02.159](https://doi.org/10.1016/j.egypro.2011.02.159)
- [35] D. Oates, P. Versteeg, E. Hittinger, and P. Jaramillo, "Profitability of CCS with flue gas bypass and solvent storage," *International Journal of Greenhouse Gas Control*, vol. 27, pp. 279–288, Aug. 2014, doi: [10.1016/j.ijggc.2014.06.003](https://doi.org/10.1016/j.ijggc.2014.06.003)
- [36] D. Li, Y. Hu, W. He, and J. Wang, "Dynamic modelling and simulation of a combined-cycle power plant integration with thermal energy storage," in *International Conference on Automation and Computing*, Huddersfield, UK, Sep. 2017, doi: [10.23919/ICoNAC.2017.8081972](https://doi.org/10.23919/ICoNAC.2017.8081972)
- [37] J. Chang, G. Lee, D. Adams, H. Ahn, J. Lee, and M. Oh, "Multiscale modeling and integration of a combined cycle power plant and a two-tank thermal energy storage system with gPROMS and SimCentral," *Korean Journal of Chemical Engineering*, vol. 38, pp. 1333–1347, Jun. 2021, doi: [10.1007/s11814-021-0789-1](https://doi.org/10.1007/s11814-021-0789-1)
- [38] V. Eveloy, P. Rodgers, and S. Popli, "Power generation and cooling capacity enhancement of natural gas processing facilities in harsh environmental conditions through waste heat utilization," *International Journal of Energy Research*, vol. 38, no. 15, pp. 1921–1936, Dec. 2014, doi: [10.1002/er.3197](https://doi.org/10.1002/er.3197)
- [39] N. Palestra, G. Barigozzi, and A. Perdichizzi, "Inlet air cooling applied to combined cycle power plants: influence of site climate and thermal storage systems," in *ASME Turbo Expo 2007: Power for Land, Sea, and Air*, no. GT2007-27046, Montreal, Canada, May 2007, pp. 583–592, doi: [10.1115/GT2007-27046](https://doi.org/10.1115/GT2007-27046)
- [40] D. R. Herber and J. T. Allison, "Nested and simultaneous solution strategies for general combined plant and control design problems," *Journal of Mechanical Design*, vol. 141, no. 1, p. 011402, Jan. 2019, doi: [10.1115/1.4040705](https://doi.org/10.1115/1.4040705)

- [41] M. Garcia-Sanz, “Control co-design: an engineering game changer,” *Advanced Control for Applications*, vol. 1, no. e18, 2019, doi: [10.1002/adc2.18](https://doi.org/10.1002/adc2.18)
- [42] A. K. Sundarajan, “Some efficient open-loop control solution strategies for dynamic optimization problems and control co-design,” M.S. Thesis, Colorado State University, Fort Collins, CO, USA, Jun. 2021. [Online]. Available: <https://hdl.handle.net/10217/233718>
- [43] J. Fernando, “Net present value (NPV),” 2021. [Online]. Available: <https://www.investopedia.com/terms/n/npv.asp>
- [44] S. J. Garrett, “Chapter 5 - sequences and series,” in *Introduction to Actuarial and Financial Mathematical Methods*. Academic Press, 2015, pp. 147–191, doi: [10.1016/B978-0-12-800156-1.00005-4](https://doi.org/10.1016/B978-0-12-800156-1.00005-4)
- [45] D. R. Herber, “Advances in combined architecture, plant, and control design,” Ph.D. Dissertation, University of Illinois at Urbana-Champaign, Urbana, IL, USA, Dec. 2017.
- [46] M. Kelly, “An introduction to trajectory optimization: how to do your own direct collocation,” *SIAM Review*, vol. 59, no. 4, pp. 849–904, Jan. 2017, doi: [10.1137/16M1062569](https://doi.org/10.1137/16M1062569)
- [47] J. T. Betts, *Practical Methods for Optimal Control and Estimation Using Nonlinear Programming*. SIAM, 2010, doi: [10.1137/1.9780898718577](https://doi.org/10.1137/1.9780898718577)
- [48] “DTQP project.” [Online]. Available: <https://github.com/danielrherber/dt-qp-project>
- [49] “linprog.” [Online]. Available: <https://www.mathworks.com/help/optim/ug/linprog.html>
- [50] New York ISO, “Energy market & operational data.” [Online]. Available: <https://www.nyiso.com/energy-market-operational-data>
- [51] J. B. Rawlings, D. Q. Mayne, and M. M. Diehl, *Model Predictive Control: Theory, Computation, and Design*, 2nd ed. Nob Hill Publishing, 2020.

- [52] G. Campos, Y. Liu, D. Schmidt, J. Yonkoski, D. Colvin, D. Trombly, N. El-Farra, and A. Palazoglu, “Optimal real-time dispatching of chillers and thermal storage tank in a university campus central plant,” *Applied Energy*, vol. 300, p. 117389, 2021, doi: [10.1016/j.apenergy.2021.117389](https://doi.org/10.1016/j.apenergy.2021.117389)
- [53] P. Falugi, E. O’Dwyer, M. A. Zagorowska, E. Atam, E. C. Kerrigan, G. Strbac, and N. Shah, *MPC and Optimal Design of Residential Buildings with Seasonal Storage: A Case Study*. Cham: Springer International Publishing, 2022, pp. 129–160, doi: [10.1007/978-3-030-79742-3_6](https://doi.org/10.1007/978-3-030-79742-3_6)
- [54] A. L. Nash, H. C. Pangborn, and N. Jain, “Robust control co-design with receding-horizon MPC,” in *American Control Conference*, 2021, doi: [10.23919/ACC50511.2021.9483216](https://doi.org/10.23919/ACC50511.2021.9483216)
- [55] A. P. Deshmukh, D. R. Herber, and J. T. Allison, “Bridging the gap between open-loop and closed-loop control in co-design: a framework for complete optimal plant and control architecture design,” in *American Control Conference*, Chicago, IL, USA, Jul. 2015, pp. 4916–4922, doi: [10.1109/ACC.2015.7172104](https://doi.org/10.1109/ACC.2015.7172104)
- [56] S. Cohen and V. Durvasulu, “NREL price series developed for the ARPA-E FLECCS program,” 2021, doi: [10.7799/1838046](https://doi.org/10.7799/1838046)
- [57] National Renewable Energy Laboratory, “National solar radiation database,” 2018. [Online]. Available: <https://nsrdb.nrel.gov>
- [58] R. Chacartegui, F. Jiménez-Espadafor, D. Sánchez, and T. Sánchez, “Analysis of combustion turbine inlet air cooling systems applied to an operating cogeneration power plant,” *Energy Conversion and Management*, vol. 49, no. 8, pp. 2130–2141, Aug. 2008, doi: [10.1016/j.enconman.2008.02.023](https://doi.org/10.1016/j.enconman.2008.02.023)
- [59] National Renewable Energy Laboratory, “Electricity annual technology baseline (ATB) data download,” 2020. [Online]. Available: <https://atb.nrel.gov/>

[60] U.S. Bureau of Labor Statistics, “Consumer price index data,” 2021. [Online]. Available:
<https://data.bls.gov/timeseries/CUUR0000SA0>

Appendix A

Case Study Parameters

A.1 NPV Economic Assumptions

Standard economic and financial assumptions used to generate the NPV results for this paper are presented in Tab. A.1 [14, 59]. All dollar values were adjusted to December 2018 dollars based on historical inflation rates as calculated by the Bureau of Labor Statistics using the Consumer Price Index [60].

Table A.1: Economic assumptions for the calculation of net present value in the case studies.

Parameter	Units	Value
L_r [59]	years	30
IRR [59]		10%
i_e [14]	%/year	3.5%
i_f [14]	%/year	2.2%

A.2 Technology Parameters

The parameters describing the technologies examined in the case studies presented in Sec. 3 are shown in Table A.2. The parameters reported reference the nomenclature of the optimization model in Sec. 2.1 and are evaluated at 15°C.

Table A.2: Techno-economic parameters for the technology configurations examined in the case studies.

Parameter	Units	B31B	ER	IPTE
ρ_f	kg NG/s/MW	0.04082	0.04082	0.04082
c_n		0.9	0.9	0.9
$\kappa_{HS,in}$	hr TES/MW	0	0.005949	0.01126
$\kappa_{CS,in}$	hr TES/MW	0	0.1609	0.1609
$\kappa_{HS,out}$	hr TES/MW	0	0.02211	0.02028
$\kappa_{CS,out}$	hr TES/MW	0	0.01986	0.02075
$\Delta\rho_f$	kg/s/MW	0	0.03783	0.03951
Δc_d		0	0.06163	0.06163
$\Delta\rho_{CO_2,in}$	kg CO ₂ /MW	0	-0.00025	-0.00026
$\Delta\rho_{CO_2,out}$	ton CO ₂ /MW	0	0.0067	0.0070
P_{CCT}, P_{CCE}	MW	0	0	0
α_C	ton CO ₂ /kg NG	0.0029	0.0029	0.0029
η^*		1	1	1
$c_{PP,VOM}$	\$/MWh	1.705	1.705	1.705
$c_{CC,VOM}$	\$/ton CO ₂	7.2	7.2	7.2
$c_{TES,VOM}^\dagger$	\$/MWh	0	0.75	0.75
$c_{PP,FOM}$	M\$/year	12.9773	12.9773	12.9773
$c_{CC,FOM}$	M\$/year	14.5360	14.5360	14.5360
$c_{HS,in,FOM}$	k\$/MW/year	0	2.5881	2.5881
$c_{CS,in,FOM}$	k\$/MW/year	0	15.0721	15.0721
$c_{HS,out,FOM}$	k\$/MW/year	0	4.12186	4.12186
$c_{CS,out,FOM}$	k\$/MW/year	0	0.79725	0.79725
$c_{HS,TES,FOM}$	k\$/hr of TES/year	0	41.9579	190.2704
$c_{CS,TES,FOM}$	k\$/hr of TES/year	0	45.5942	56.9928
C_{PP}	M\$	537.7230	537.7230	537.7230
C_{CC}	M\$	743.6010	743.6010	743.6010
$c_{HS,in}$	k\$/MW	0	64.7012	39.3198
$c_{CS,in}$	k\$/MW	0	376.8015	376.8018
$c_{HS,out}$	k\$/MW	0	103.0466	30.3505
$c_{CS,out}$	k\$/MW	0	19.9311	20.8169
$c_{HS,TES}$	M\$/hr of TES	0	1.048947	4.756760
$c_{CS,TES}$	M\$/hr of TES	0	1.139856	1.424820
\bar{P}_{PP}	MW	634.741	634.741	634.741
$\bar{P}_{HS,in}$	MW	0	840.515	443.9915
$\bar{P}_{CS,in}$	MW	0	31.06755	31.06755
$\bar{P}_{HS,out}$	MW	0	45.2353	49.303
$\bar{P}_{CS,out}$	MW	0	50.3432	48.2011

* η is for ($\eta_{GE}, \eta_{HS}, \eta_{CS}$)

[†] $c_{TES,VOM}$ is for ($c_{HS,VOM}, c_{CS,VOM}$)

Appendix B

Extended Time Horizon Visualizations

Figures B.1–B.4 show 20 days of continued operation extracted in each of the 4 seasons and visualize more of the control solution trajectories extracted from the optimization of a full year of operation in the “BaseCaseTax” market scenario presented by GenX [19]. The HS technology examined is resistive heating with 4 hours of equivalent TES capacity and nominal energy transfer rates, and vapor compression is the CS technology with 2 hours of equivalent capacity. Recall that in the simultaneous case, all 365 days are optimized all-at-once, not just the 20 day snippets shown here.

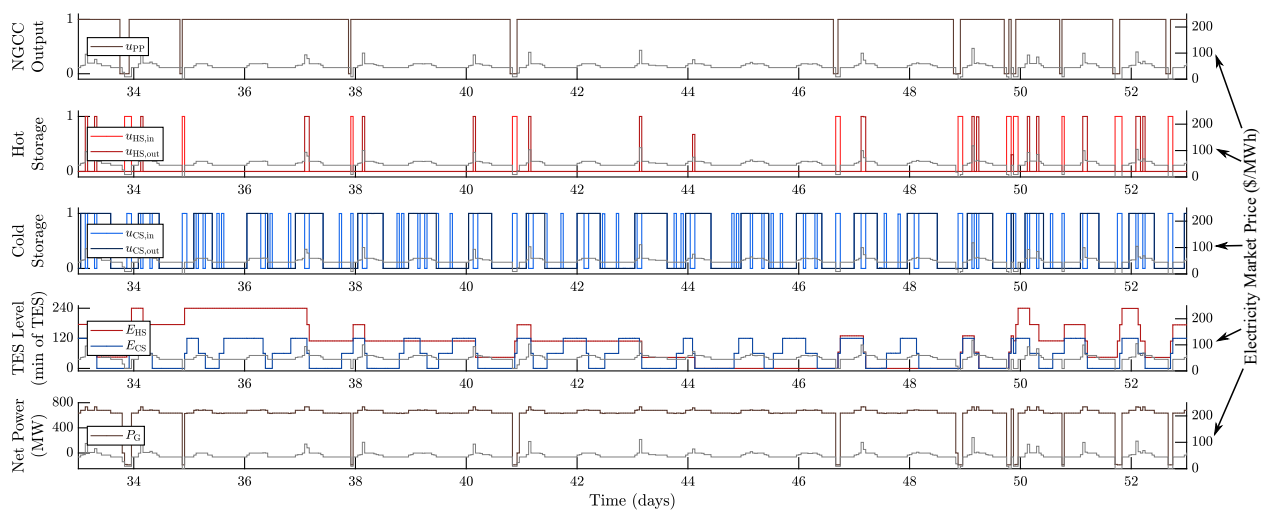


Figure B.1: Control signals for optimal TES operation for 20 days in February.

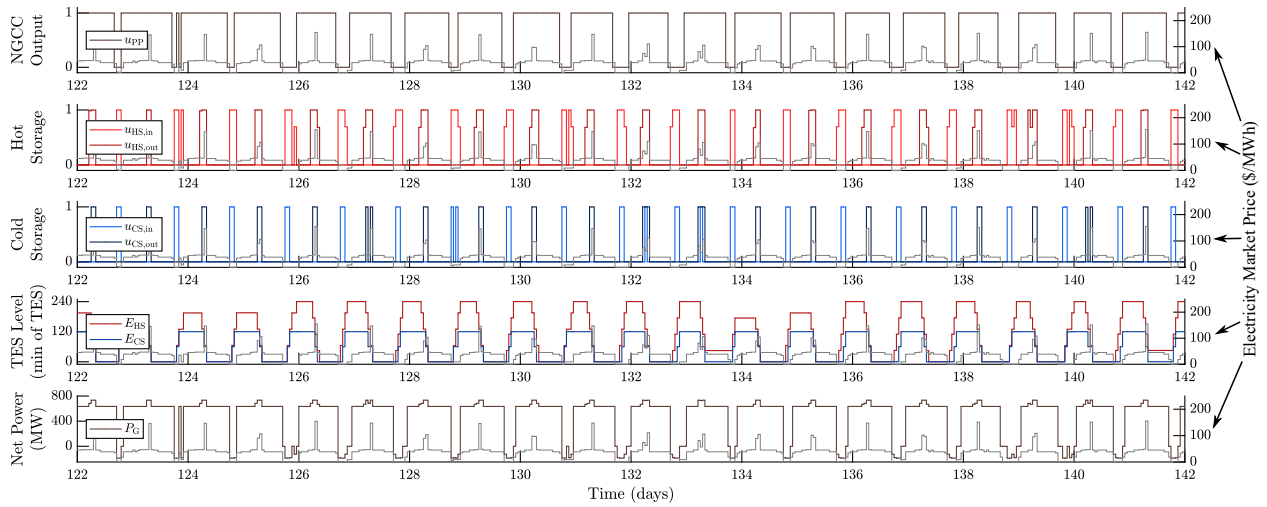


Figure B.2: Control signals for optimal TES operation for 20 days in May.

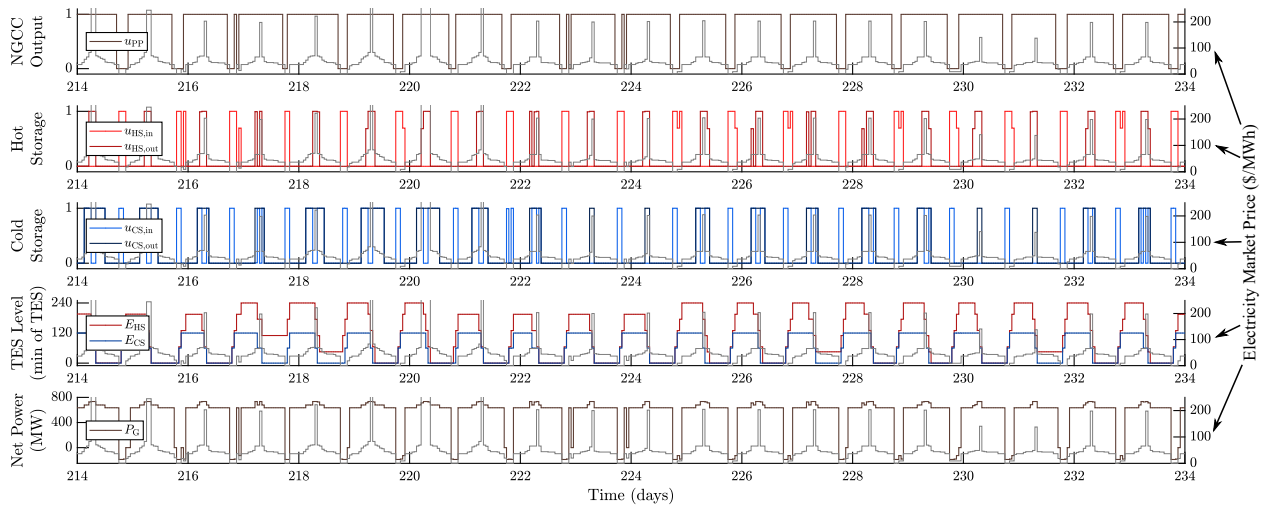


Figure B.3: Control signals for optimal TES operation for 20 days in August.

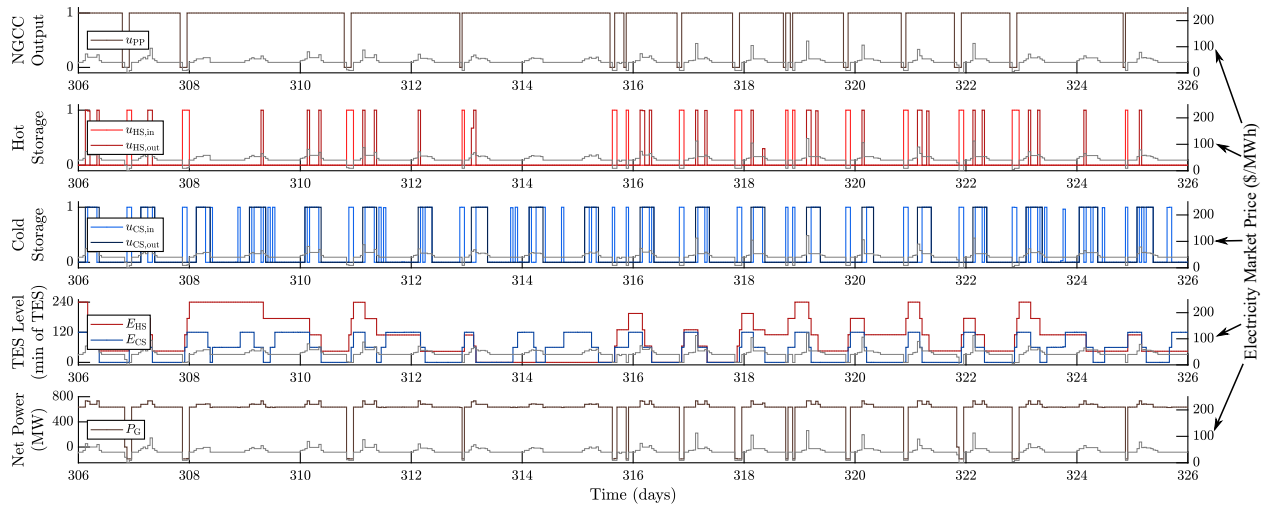


Figure B.4: Control signals for optimal TES operation for 20 days in November.